Applied Geochemistry 118 (2020) 104609

Contents lists available at ScienceDirect

Applied Geochemistry

journal homepage: http://www.elsevier.com/locate/apgeochem

Noble gas as a proxy to understand the evolutionary path of migrated CO_2 in a shallow aquifer system

YeoJin Ju [a], Seong-Sun Lee [a], Dugin Kaown [a], Kang-Kun Lee [a,*], Stuart M.V. Gilfillan [b], Doshik Hahm [c], Keyhong Park [d]

[a] School of Earth and Environmental Sciences, Seoul National University, 1 Gwanak-ro, Gwanak-gu, Seoul, 08826, South Korea
[b] School of GeoSciences, The University of Edinburgh, Grant Institute, James Hutton Road, Edinburgh, EH9 3FE, UK
[c] Department of Oceanography, Pusan National University, Busan, South Korea
[d] Division of Polar Ocean Science, Korea Polar Research Institute, Incheon, South Korea

ARTICLE INFO

Editorial handling by Prof. M. Kersten

Keywords:
Carbon capture and storage
CO_2 leakage
Noble gas tracing
Degassing
Inherent tracer
Monitoring

ABSTRACT

To provide confidence in the safety of a carbon capture and storage (CCS) project, researchers have focused on developing monitoring techniques to trace the unlikely, but potentially possible, migration of CO_2 from a deep reservoir. Among the various techniques, noble gas tracing is a beneficial approach, owing to the unique noble gas fingerprints present in injection fluids, the deep reservoir, and the shallow aquifer above the storage area. However, the value of this approach has been limited to demonstrations in a natural analogue CO_2-rich reservoir and an artificial injection test site. Therefore, further efforts are required to link those valuable observations to an actual CCS site. In this study, we outline how to use these tracers for actual monitoring work in a shallow aquifer system. First, two artificial injection tests were performed using He, Ar, Kr, and SF_6 to understand the behavior of the leaked plume in the shallow aquifer system. In both tests, the noble gas ratio remarkably changed with the solubility-controlled process and the mixing process. To extend and link the valuable findings from the artificial injection tests to an actual CO_2 leakage event, we performed a leakage simulation using data from a real CO_2 injection site, i.e., the Weyburn–Midale site. This simulation suggested that combinations of ^4He with other heavier noble gases can be used to monitor CO_2 leakage, as they allow us to separate and explain the major interactions governing the migration of the leaked plume in the shallow aquifer system. Additionally, although the high CO_2 density of a dissolved plume is known to add uncertainty in quantitative approaches, the influence of those effects was negligible when compared to the errors arising from the wide variation in the noble gas fingerprints in the leaked CO_2. This study, therefore, provides insight into the evolutionary path of the migrated CO_2 plume in the shallow aquifer system and to the results can be used to inform the tracing of a leakage source within a shallow aquifer despite various mechanisms complicating the plume distribution.

1. Introduction

A carbon capture and storage (CCS) project uses an impermeable or low-permeability cap rock to trap sequestered CO_2 in a formation without leakage. The CO_2 injected into the storage formation is sequestrated by subsurface trapping mechanisms, namely structural/stratigraphic trapping, residual trapping, solubility trapping, and mineral trapping mechanisms. Evidence shows that these are effective on a geologic time scale (Alcalde and Flude et al., 2018; Altman et al., 2014; IPCC, 2005). However, a recent event where artificial injection activity of water in an enhanced geothermal system (EGS) triggered a 5.5 magnitude earthquake in Pohang, South Korea (Lee et al., 2019) led to increased public awareness of the potential issues of injecting fluids into the subsurface in Korea. This situation led to the temporary closure of a CO_2 capture and storage demonstration project intended to be performed in the Pohang Basin, South Korea (Chen et al., 2018). Furthermore, it was alleged that CO_2 that had leaked from the storage formation at the Weyburn-Midale site had polluted a nearby shallow groundwater zone (Beaubien et al., 2013). These examples highlight the need for a robust monitoring regime of any future geological storage site to provide

* Corresponding author.
E-mail addresses: jinee18@snu.ac.kr (Y. Ju), soon3311@snu.ac.kr (S.-S. Lee), dugin1@snu.ac.kr (D. Kaown), kklee@snu.ac.kr (K.-K. Lee), stuart.gilfillan@ed.ac.uk (S.M.V. Gilfillan), hahm@pusan.ac.kr (D. Hahm), keyhongpark@kopri.re.kr (K. Park).

https://doi.org/10.1016/j.apgeochem.2020.104609
Received 6 October 2019; Received in revised form 18 January 2020; Accepted 20 April 2020
Available online 28 April 2020

reassurance that CO_2 is being safely stored and that any migration from the site can be detected.

The monitoring of leaked CO_2 is often complicated by naturally occurring CO_2 in the subsurface system. The distribution of CO_2 is very heterogeneous in a natural groundwater system as a result of chemical, biological, and physical interactions (Risk et al., 2015). The use of stable C isotopes for leakage monitoring can also be challenging because their signals in leaked fluids can overlap with those of common surface sources (e.g., landfills) (Györe et al., 2017), following bacterial activity that enriches the ^{13}C by an oxidation process (Whiticar et al., 1999). However, noble gases are chemically and biologically inert, and are only affected by quantifiable physical processes in a shallow aquifer system. Therefore, noble gases can provide a means to separate and explain the physical processes in a biochemically complicated system (Kilgallon et al., 2018). The benefits of this tracer were first recognized in an enhanced oil and recovery (EOR) site, where engineers used this particular characteristic of noble gases to explain the physical process of a solubility-controlled mechanism in a multi-phase system composed of gas, water, and oil phases (Bosch and Mazor, 1988; Ballentine et al., 2002; Prinzhofer, 2013). In this complex system, the noble gases were phase-partitioned at the materials' interfaces, and the noble gas compositions were mass-dependently fractionated according to their solubilities (Ballentine et al., 1991, Ballentine and O'nions, 1994; Lollar et al., 1997; Pinti and Marty, 1995). These valuable techniques have now been extended to the study of CCS projects to monitor the migration of a multiphase CO_2 plume in the subsurface system.

Although noble gases have been actively applied in CCS research for various purposes (Myers et al., 2013), they have been largely used to identify CO_2 migration from a deep reservoir into a shallow aquifer to define a preferential pathway of migrated CO_2 and to resolve the physical interactions governing the fate of the CO_2-rich plume.

Noble gases have been used to trace CO_2 leakage in natural analogue sites and artificial injection experiments. Lafortune et al. (2009) suggested the potential applicability of noble gas for tracing gas leakage from a reservoir into a shallow groundwater system, as the reservoir has a signature of this tracer that is distinguished from that of shallow-depth groundwater. This was clearly proven at a natural analogue site of post-emplacement seepage. For example, Gilfillan et al. (2011) concluded that an elevation of HCO_3^- in shallow-subsurface and surface waters originated from deep reservoir leakage, based on a fingerprint of high-crustal ^4He. Györe et al. (2018) also pointed out that high ^4He in a deep reservoir can be used as a potential fingerprint to trace the fugitive release of reservoir gas. The concept of a noble gas fingerprint was extended to tracer-enhancement work for artificially injected CO_2 at the Cooperative Research Centre for Greenhouse Gas Technologies (CO2CRC) Otway Project to produce a strong signal for CO_2 plume leakage by distinguishing artificial CO_2 from natural CO_2 (Stalker et al., 2015).

In order to better understand the pathway of migrating CO_2 within a deep reservoir, several artificial injection experiments have been undertaken. For example, CO_2 gas was injected into a heterogeneous hydrocarbon reservoir (~3080 m deep) within the Tuscaloosa Formation reservoir, Mississippi, United States, and was followed by continuous monitoring (Lu et al., 2012). This resulted in a unique bumpy breakthrough of noble gas having multi-peaks suggesting the existence of preferential paths between a leakage point and monitoring wells (Lu et al., 2012). In a shallow depth vadose zone injection test, preferential paths were found between the injection point and monitoring probes, as induced by the natural heterogeneity of the limestone at the DEMO-CO_2 project, France (Rillard et al., 2015). Lighter noble gases (He and Ne) were more helpful in defining the preferential path in the vadose zone than CO_2 and other tracers as they have faster arrival times at the monitoring probes owing to their higher diffusion coefficients and lower solubility within the soil water in the CO_2-Vadose project, France (Cohen et al., 2013).

Detailed and extensive research on the fate of CO_2 has been undertaken in natural CO_2-rich reservoirs, which serve as analogues for artificial CO_2 storage. For example, Zhou et al. (2005) constrained the evolution of natural CH_4 and CO_2 based on the mass-dependent fractionation of noble gases in a coalbed methane system. Studies on a natural analogue site of a deep CO_2 storage reservoir suggested that a multi-step solubility-controlled process was significantly involved in the fate of CO_2 gas under the impermeable cap-rock, as explained by the deeply fractionated noble gas ratio (Gilfillan et al., 2008; Zhou et al., 2012). Then, Gilfillan et al. (2009) concluded that naturally injected CO_2 has been primarily sequestrated within deep reservoirs through a solubility-controlled mechanism. In an engineered CO_2 injection site, Györe et al. (2015) and Györe et al. (2017) observed that the noble gas composition of produced gas can be successfully used to constrain the fate of the sequestrated CO_2 at the Cranfield enhanced oil recovery (EOR) field and identified a clear sink of free-phase CO_2 in areas making contact with the reservoir groundwater. A numerical model has also been applied to define the fate of a reservoir of CO_2 by identifying the budget of residual trapped and immobilized gas in a deep storage site at the CO2CRC Otway test injection site (LaForce et al., 2014). Moreover, Zhang et al. (2011) delineated that immobilized gaseous CO_2 retards the arrival of noble gas tracers, owing to their preferential partitioning into CO_2 bubbles at interfaces. In a recent artificial injection experiment, an attempt was made to understand the fate of artificial CO_2 released into a shallow groundwater system (Ju et al., 2019), where the fate of the leaked CO_2 was constrained using noble gases. This highlighted the importance of solubility control and mixing mechanisms in shallow-depth groundwater.

Recently, studies have begun applying a noble gas fingerprinting tool for an actual monitoring purpose, i.e., to trace leaked CO_2 from a reservoir into a shallow aquifer system. The noble gas tracing in the shallow system is based on the inherent compositional difference between the reservoir fluid and the groundwater above, and the composition of injected CO_2 is dependent on various CO_2 capture mechanisms (Flude et al., 2016). Gilfillan et al. (2017) recognized the usefulness of composition at a real CO_2 injection site. For example, the storage reservoir was two orders of magnitude richer in radiogenic ^4He compared to normal soil gases, providing an opportunity to evaluate allegations that unplanned migration of CO_2 into a shallow aquifer near the Weyburn Midale oil fields had taken place.

Although noble gases have proved useful for tracing a CO_2 plume in many sites as described above, to the best of our knowledge, it has not yet been extensively used for monitoring in a shallow aquifer (Lee et al., 2016). Moreover, most works have been limited to artificial release experiments and natural analogue sites, implying that further efforts are still required to link the valuable previous observations to an actual CCS site. Therefore, this study attempted to discuss the application of these tracers to the monitoring of actual unplanned CO_2 migration from a CCS site. For this purpose, two injection tests were completed in a shallow aquifer system using noble gas tracers. This was intended to explain the major processes responsible for the fate of the migrated CO_2 plume in a multi-phase state and to verify the findings from previous research. Then, based on the observations, we simulated the CO_2 leakage by using analytical solutions and discussed how to use noble gas to identify CO_2 migration, and to constrain the fate of the migrated CO_2.

2. Material and methods

2.1. Artificial injection test

Sequestrated CO_2 can be mobile when the cap-rock is broken or damaged (Fig. 1). Then, portions of free-phase CO_2 move upward due to buoyancy forces. Accidental leakage can occur through various vertical conduits such as an injection well, abandoned wells, or natural faults over different periods of time (e.g., continuous low level leakage or short duration blowouts) (Alcalde and Flude, 2018). While the free-phase CO_2 migrates through conduits, it can spread into the multiple layers

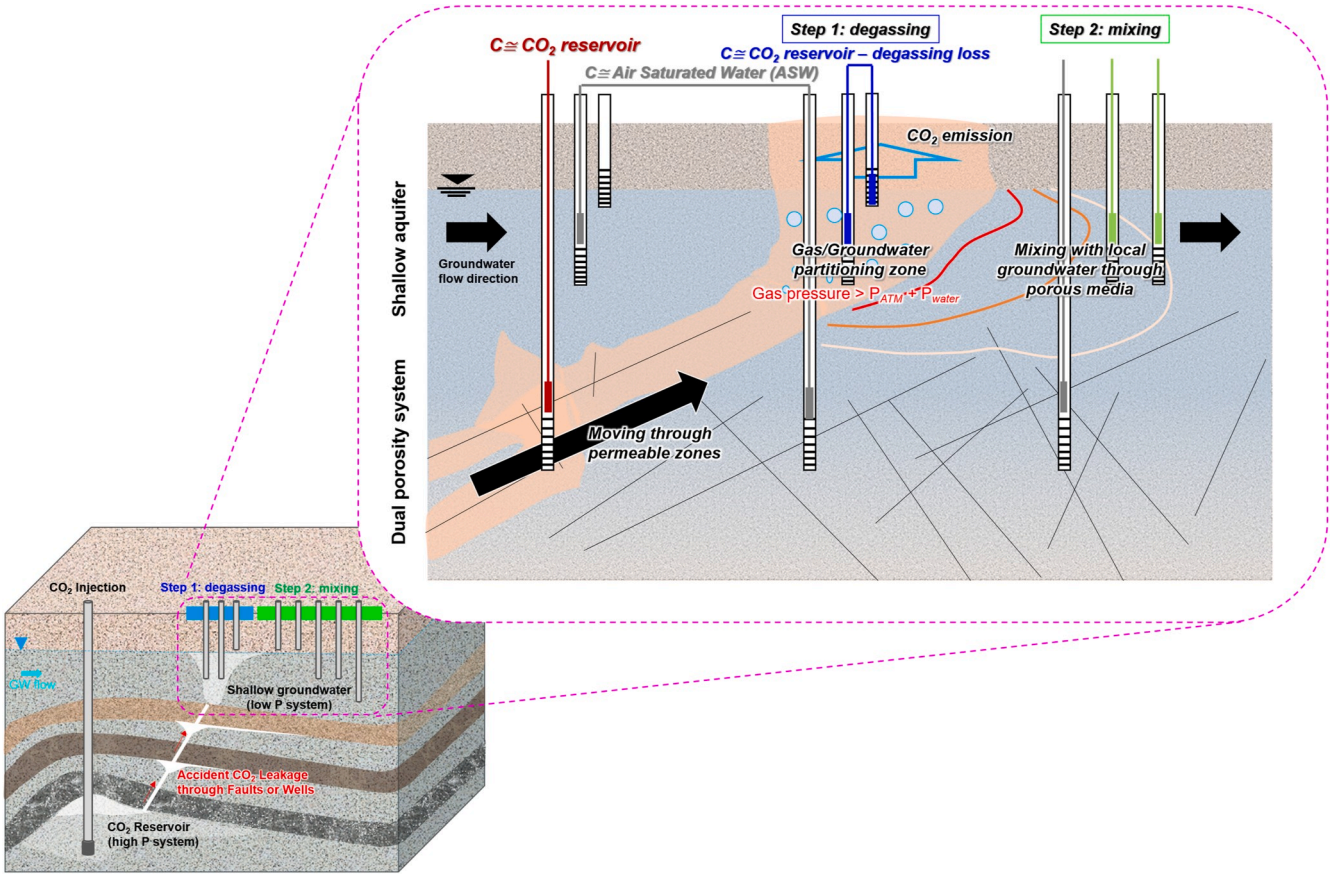

Fig. 1. Conceptual figure to demonstrate accidental CO_2 leakage from a deep reservoir into a shallow groundwater system. Early-stage fate of CO_2 is primarily controlled by the solubility-controlled process (i.e., degassing) due to a high gas pressure.

splitting the mass (Jung et al., 2015) (Fig. 1). Among the multiple layers, the ones with lower-permeabilities act as a barrier preventing the CO_2 from reaching a shallower aquifer. Following a series of stratigraphic trappings, some volumes of CO_2 finally reach the lower pressure system of shallow groundwater, which is the very portion discussed throughout this paper (see Fig. 1).

The two artificial injections were performed to demonstrate the accidental leakage of CO_2 into the shallow aquifer. In particular, the injection experiments focused on the early-stage fate of free-phase CO_2 reaching the low-pressure system (i.e., shallow aquifer). The initial state of CO_2 is characterized by a high partial pressure that can naturally nucleate the bubbles (Fig. 1). The degassing dominantly occurs around a leakage point until stabilization occurs in the low-pressure system. After the degassing, the CO_2 bubbles are redistributed between the groundwater (dissolved and remaining budget) and the atmosphere (degassed and lost budget), reducing the total migrated CO_2 budget. The initial degassing is very important because it controls the overall budget of CO_2 remaining in the subsurface after it migrates into a shallower system (Ju et al., 2019). In this context, the two experiments, in which gas-charged groundwater was injected into a shallow aquifer, were performed to demonstrate the early-stage solubility-controlled process (i.e., degassing).

2.2. Test site overview

The first injection test was conducted in Wonju, Korea (figure. 2). The aquifer at the study site consists of weathered and highly fractured Jurassic biotite granite overlain by soil and alluvial deposits (Yu et al., 2006; Baek and Lee, 2011). The single-well tracer test (SWTT) was performed in the alluvial deposits, which are a uniform material without fractures and conduits. The aquifer thickness was 10–15 m. The aquifer hydrology at the site had a wide range of seasonal and spatial variations. The observed water table was 2–13 m below the ground surface, but remained below 11 m during the dry season, when the pilot test was performed. The hydraulic gradient varied from 0.008 m to 0.023 m. A pumping and slug test revealed that the hydraulic conductivity of the site ranged between 2.0×10^{-4} cm/s and 4.2×10^{-3} cm/s. In addition, the flow velocity of the regional groundwater was estimated, using ^{3}H–^{3}He analysis, to vary from 1.9×10^{-6} to 1.2×10^{-4} m/s (Kaown et al., 2014). A detailed description of the geologic features, seasonal variations in aquifer hydrology, and land-use history of the study site can be found in Lee et al. (2015).

The second injection and recovery test was completed at the Korea CO_2 Storage Environmental Management (K-COSEM) experimental test site in Eumseong, Korea (Fig. 3). A monitoring network was established at the test site for the CO_2 release and monitoring experiments. Geological information was collected from borehole data at the study site: an alluvial deposit was found occurring 0–2 m below ground level (b.g.l.), weathered soils were found 2–30 m b.g.l., weathered rocks were found 30–70 m b.g.l., and bedrock was found > 70 m b.g.l. (Ju et al., 2018a). The host rock was dark gray or light gray biotite granite. The inter-well tracer test (IWTT) was performed in the weathered soils zone regarded as a uniform material without any fractures and conduits. The water table was 16–17 m b.g.l., and the hydraulic gradient ranged from 0.01 to 0.05. The regional flow direction was from northwest to southeast. The hydraulic conductivity estimated from the pumping test ranged from 4.0×10^{-6} m/s to 2.0×10^{-5} m/s. A push-and-pull test was performed to identify the groundwater linear velocity (0.06–0.44 m/d), effective porosity (0.02–0.23), and uppermost aquifer thickness (47 m) of the study site. Detailed discussions on the sequential hydraulic tests

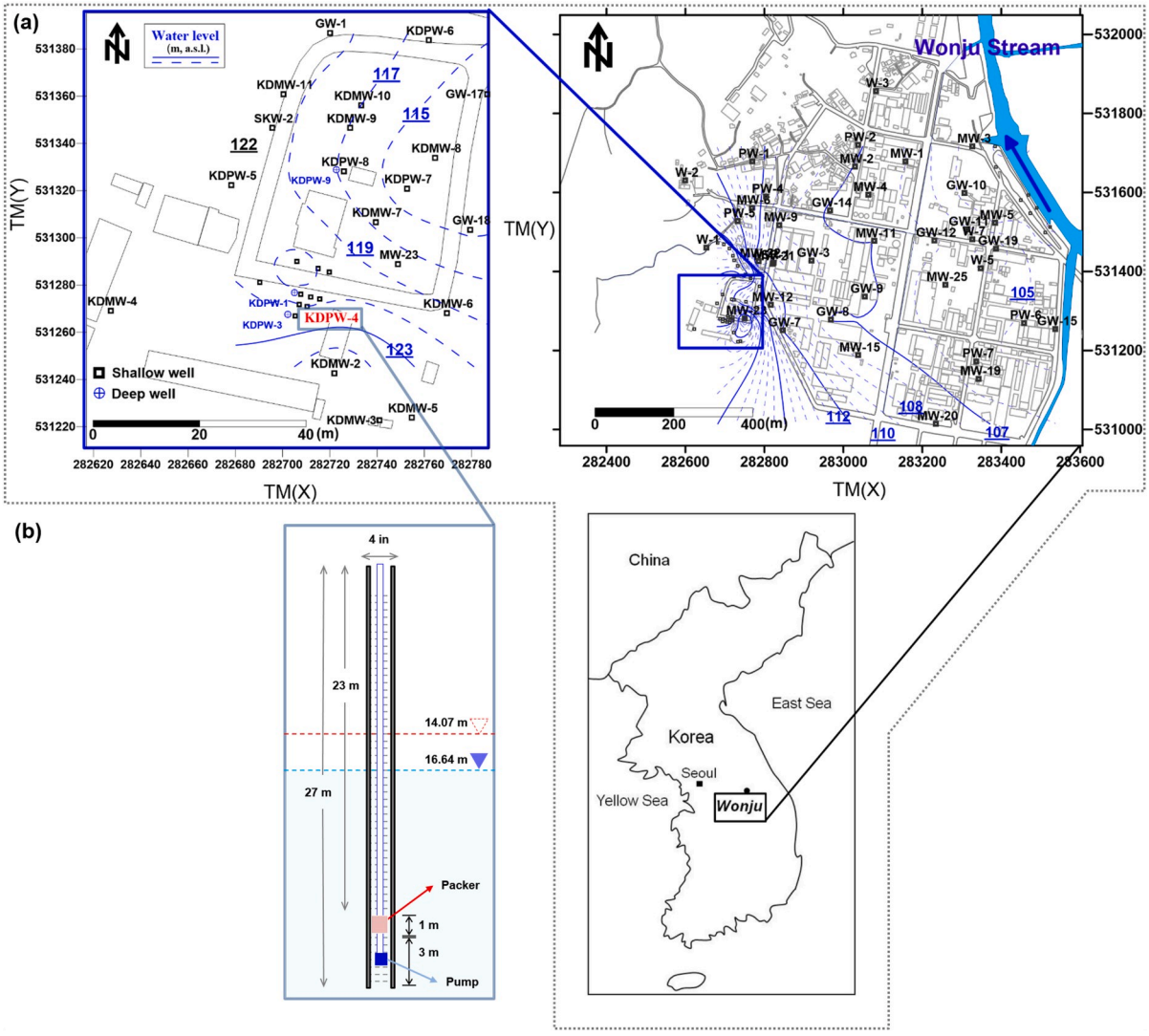

Fig. 2. (a) Site map of Wonju, Korea; (b) full-screened KDPW4 was used for the SWTT at the site. Injection was completed 24–27 m below the ground surface and approximately 10 m below the water table. The injection interval was isolated using packer during the SWTT. The water table inside the interval changed from 14.07 m (i.e., red triangle) to 16.64 m (i.e., blue triangle) below the surface during the pull-phase of SWTT. (For interpretation of the references to color in this figure legend, the reader is referred to the Web version of this article.)

for establishing the monitoring network at the K-COSEM experimental test site are summarized in Lee et al. (2017) and Lee et al. (2018).

2.3. Experimental design overview

Tracer-mixed groundwater was prepared and artificially injected into the groundwater. First, each sample of tracer-infused groundwater was created by flowing inert gases into local groundwater using a gas regulator, ball-flowmeter, flexible tube, silencer (for gas diffusion), and carboy bottle (Fig. 4). The volumes of gas-charged groundwater samples were gently mixed together in the order of their solubility in groundwater (i.e., Kr → Ar → He). The injection was completed using a submersible and controllable quantitative pump "MP1" (Grundfos, Bjerringbro, Denmark). The sample for the injection fluid (C_0) was collected during the injection period, and the salinity was measured at the sampling time using portable equipment from Yellow Springs Instruments (YSI) (YSI Inc./Xylem Inc., USA). The salinity was reported in units of ppt, with a precision of ±0.01 ppt.

The first pilot test was carried out in Wonju, Korea, as a single-well tracer test (SWTT). The SWTT is a three-step process consisting of push, drift, and pull periods. During the push period, gas-charged groundwater (200 L) composed of salt, Ar, He, and SF_6 was injected, and was followed by the release of a chaser fluid (120 L) to flush the residual volume of injection water from the injection wellbore. The injection speed was 9.30 L/min (September 22, 2016) using KDPW4 as the injection well. This is a fully screened well with a depth of 27 m (Fig. 1). The target injection zone was 24–27 m below ground level, and 10 m below the water table. A packer was used to tightly seal the area 1 m above the target injection zone. After the injection period, the tracer-infused water had a drift time of 1522 min in the groundwater system. Then, in the pull period, it was recollected for 319 min at a rate of 3.87 L/min through the injection well (September 23, 2016). At the same time, parts of the pulled groundwater were sampled at the well surface. The samples of the inert gas tracers were collected at 2–10 min intervals that were gradually increased. The salinity was measured *in situ* using portable equipment from YSI (YSI Inc./Xylem Inc, USA) every 2–10 min, and this interval was also gradually increased.

The second pilot test was performed at the K-COSEM experimental test site as an inter-well tracer test (IWTT). Before the tracer injection, an induced hydraulic gradient of 0.93 was created between the injection well (IW) and saturated zone monitoring well (SMW) 2–3 (Fig. 3). Gas-charged groundwater (1000 L) composed of salt, Kr, Ar, and He was

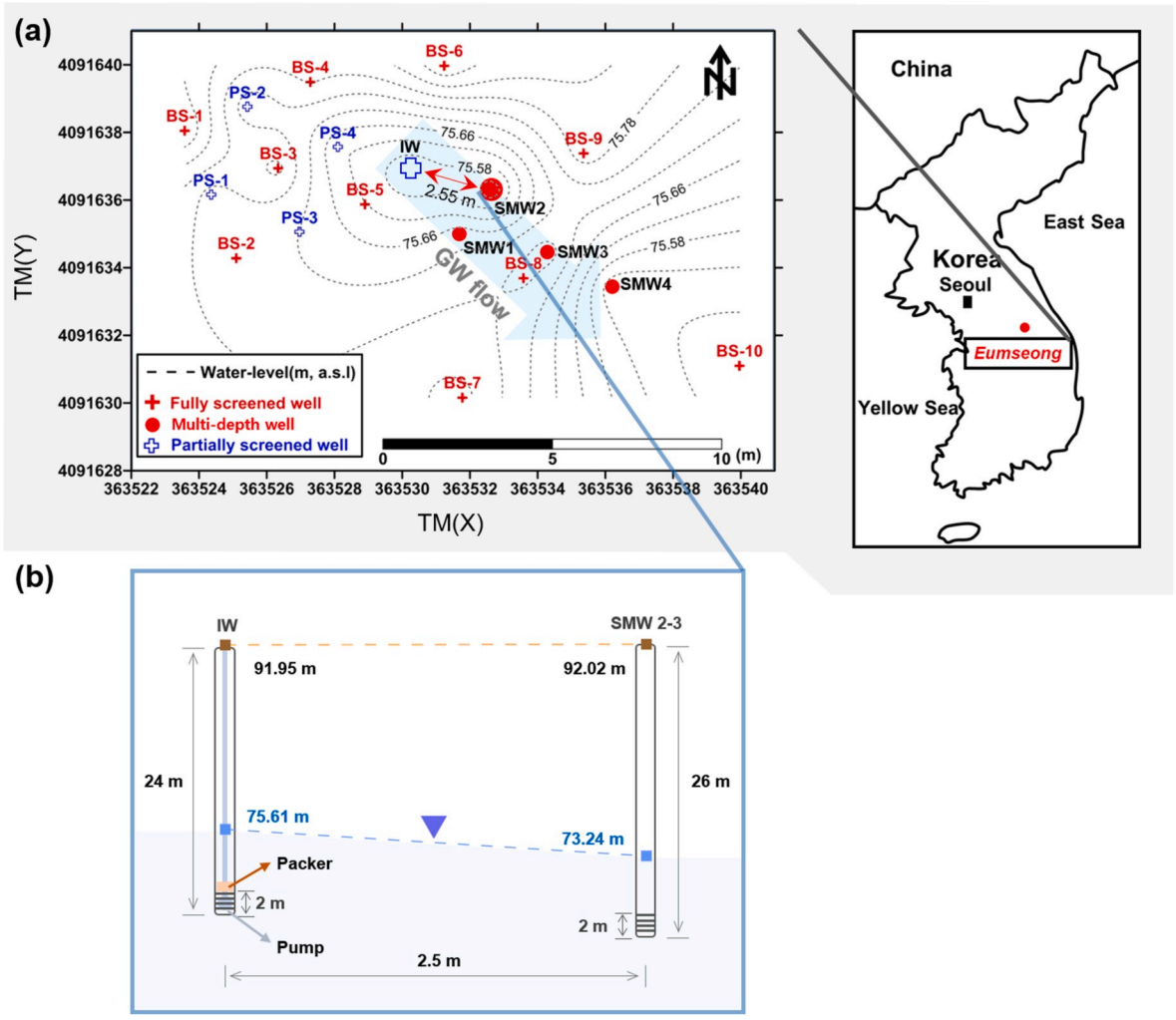

Fig. 3. (a) Site map of Eumseong, Korea. (b) Injection well (IW) and saturated zone monitoring well (SMW) 2–3 were used for the IWTT. The injection was completed 21–24 m below the ground surface and 4.5–7.5 m below the water table. Injection fluid moved along an induced pressure gradient of 0.93 between the two wells.

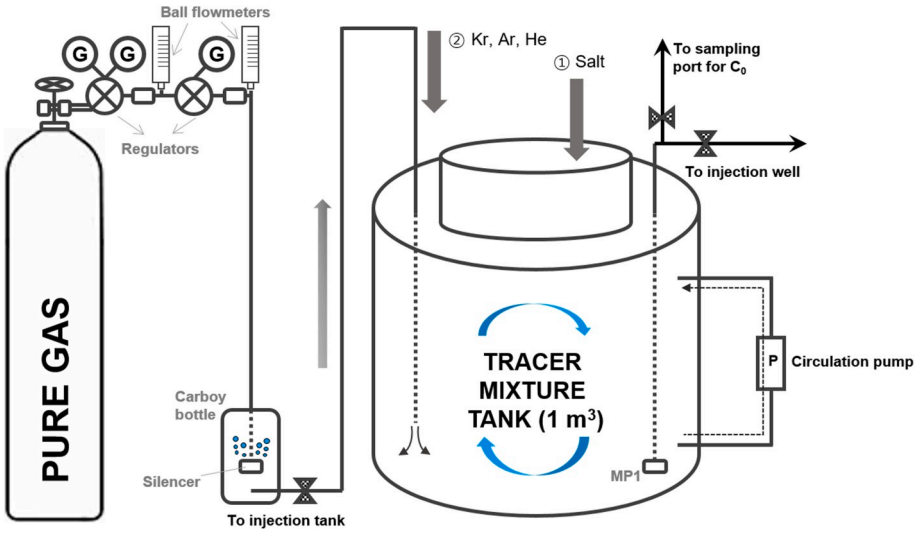

Fig. 4. Schematic figure of the injection system. Volumes of tracer-infused groundwater were first prepared by blowing a pure gas (He, Ar, Kr of 99%) into the local groundwater; then, the gas-charged water samples were gently mixed together in a closed tank with a circulation pump until they were injected into the groundwater system. The injection fluid (C_0) was sampled at the sampling port attached to this tank during the injection period.

released into the IW at a rate of 4.74 L/min (October 13, 2016). The target injection zone was 21–24 m below the ground surface, and 4.5–7.5 m below the water table at IW. The injection event was followed by 10 days of monitoring at the SMW 2–3 of down gradient (to October 22, 2016). Parts of the pulled groundwater were sampled at the well surface of SMW 2–3. The samples for the inert gas tracers were collected in 2–5 h intervals that were gradually increased. The salinity was measured *in situ* using portable equipment from YSI (YSI Inc./Xylem Inc, USA) every 2–5 h, and this interval was also gradually increased.

2.4. Data acquisition from water samples

The groundwater samples for sulfur hexafluoride (SF_6) were collected in glass bottles and were tightly sealed using caps with metal liners. The sample analysis was automatically completed at the Core Laboratory of Innovative Marine and Atmospheric Technology (CLIMATE) at the Pohang University of Science and Technology (POSTECH). The automatic device included a gas chromatograph equipped with an electron capture detector, a SF_6-extraction device, a global positioning system, and a data acquisition system based on Visual Basic 6.0/C 6.0. The SF_6 in the groundwater was quantified in comparison to gas standards of 6, 60, 103, 104, 200, 352, and 704 pptv. The precision of this method was better than 0.2% (Koo et al., 2005).

For noble gas analysis, 28 cm^3 of groundwater was sampled using a copper tube and a stainless-steel clamp (to prevent air contamination). The samples were analyzed in the noble gas analysis laboratory at the Korea Polar Research Institute (KOPRI). First, the dissolved gas was extracted from the groundwater under a high vacuum ($\sim 10^{-7}$ mbar) and stored in an aluminosilicate ampoule to remove the majority of the water in a manner similar to the method of Lott and Jenkins (1998). The extracted gas was further treated using a separated and automated processing line equipped with cryogenic traps and getter pumps (hot and cold St 101, SAES) (Beyerle et al., 2000) as outlined in Stanley et al. (2009) to remove residual water vapor, active gases, and other condensable gases. Then, each noble gas component was cryogenically separated and drawn down into a mass spectrometer, i.e., a residual gas analyzer (RGA) 200 (Stanford Research Systems, California, USA), from low mass to high mass. ^4He, ^{40}Ar, and ^{84}Kr were quantified and calibrated against air standards of 0.9–2.7 cm^3 in consideration of the wide concentration range of artificially enhanced tracers. Then, the abundant isotopes were reported as the total amount of each noble gas at standard temperature and pressure (STP), assuming they are isotopically air-like. The analytical error for the post-injection data was less than 5% based on duplicate sample analyses (Ju et al., 2018b, 2019).

3. Results

3.1. Tracing artificially leaked plume

The noble gas tracer method has shown the potential to explain the fate of high-pressure CO_2 that has migrated from a deep reservoir into a shallow aquifer system (Gilfillan et al., 2017; Ju et al., 2019). In this section, the behavior of the noble gas was determined following the two separate controlled release experiments in the shallow-depth aquifer system. Specifically, during the two injection tests, the mass recovery was observed after injecting the groundwater charged with the partitioning (i.e., inert gas tracers) and non-partitioning tracers (i.e., salt) into the shallow aquifers. Here, the partitioning tracer is defined as a substance having a partitioning behavior in a multi-phase system composed of gas and groundwater and, the non-partitioning tracer only exists as a dissolved phase in the multi-phase system.

3.1.1. Mass recovery curve of the leaked plume

A total of 200 L of groundwater (C_0) containing 68.6 ppb of SF_6, 2.05 $\times$ 10^{-6} cm^3 STP/g of He, 3.06 $\times 10^{-3}$ cm^3 STP/g of Ar, and 10.7 ppt of salt was injected into the shallow aquifer. The mass recovery of the inert gas tracers was calculated in an identical manner as Kim et al. (2018), where the total recovery was a summation of the areas in a volume-concentration plot (i.e., recovery = Σ volume (L^3) $\times$ concentration (M/L^3)). The results revealed that the recovery ratio of each tracer was clearly related to its respective solubility. As shown in Fig. 5a, the recovery ratios of SF_6, He, Ar, and salt were 49.3%, 58.1%, 78.2%, and 73.1%, respectively. The solubility-controlled processes of phase-partitioning and degassing influenced the fate of the injected gas tracers as expected (Ballentine et al., 2002). The tracer recovery ratios from single-well push-pull tracer tests exhibited various ranges of distribution depending on the nature of tracers, drift time, pump back rate, and density effect, and several controlled tests revealed that the recovery ratios do not reach 100% (Kim et al., 2018). Although salt is known to be conservative in a groundwater system, the mass recovery of salt was slightly less than that of the Ar tracer. As salt does not undergo phase-partitioning in a groundwater system, entrapment of salt mass into low permeability zones was a possible reason for the mass loss in the SWTT (Kim et al., 2018, 2019).

A total of 1000 L of groundwater containing 4.02 $\times$ 10^{-6} cm^3 STP/g of He, 2.29 $\times$ 10^{-2} cm^3 STP/g of Ar, 1.05 $\times$ 10^{-5} cm^3 STP/g of Kr, and 5.87 ppt of salt was injected into the shallow aquifer. The mass recovery rate of the IWTT was much lower than that of the SWTT. In particular, the difference between the non-partitioning tracer (i.e., salt) and the partitioning tracers (i.e., noble gas tracers) in terms of mass recovery was much greater than that of the SWTT, in which the mass recoveries of He, Ar, Kr, and salt were 0.0135%, 0.0137%, 0.0602%, and 75.0%, respectively (Fig. 5b). The non-partitioning tracer flows along the groundwater flow paths, and only a portion of the tracer mass is not captured in the recovery well because of dispersion or density-effect (Kim et al., 2018). In contrast, the partitioning tracers can easily escape from the flow paths, owing to their high diffusivity and partitioning behavior (Carrigan et al., 1996; Heilweil et al., 2004), resulting in a significant decrease in the mass recovery (see next section). Specifically, the extremely low level of recovery for the noble gas tracers, which was three orders of magnitude lower than that of salt, seems to be attributable to several factors related to the design of the experiment: 1) the brine had been charged with insoluble tracers for several hours; therefore, it is possible that the total gas pressure of injected water increased beyond $P_{ATM} + P_{H2O}$ at the injection point, resulting in active bubble growth; 2) the pumping action at the extraction well (i.e., SMW 2–3) possibly induced a pressure drop, accelerating the bubble growth; 3) the upward movement of the injected plume toward the water table through the permeable materials of the borehole resulted in a re-equilibrium of the high P plume (i.e., gas-charged water) with the atmosphere. Ide et al. (2006) highlighted the degassing mechanism of a high P plume through borehole materials in detail. The mass recovery ratios of the partitioning tracers, however, were clearly in the order of their solubilities for groundwater (Table A1 in Appendix A). Therefore, solubility-controlled processes influenced the fate of the gas-charged plumes during the IWTT (Ballentine et al., 2002).

3.1.2. Fate of the leaked plume

In the mass recovery curves, the recovery ratios of the noble gas tracers followed the order of the tracers' solubilities in groundwater, suggesting that solubility-controlled processes influenced the migration of the leaked plume. The Rayleigh distillation equation was used to explain the influence of the solubility-controlled processes on the fate of the leaked plume (Ballentine et al., 2002). The equations for estimating the degassing process are listed in Appendix A, where the partitioning coefficients in pure water system were adopted for the calculation (Table A1). A continuous degassing of the He and Ar tracers is apparent, as shown in Fig. 6 (i.e., the gray arrow). Without the degassing loss, the tracers were expected to follow the mixing line between the injection and background concentration (i.e., the dashed line for Fig. 6a and dash-dot line for Fig. 6b). However, once the degassing process starts, the noble gas composition of the dissolved plume fractionates, because

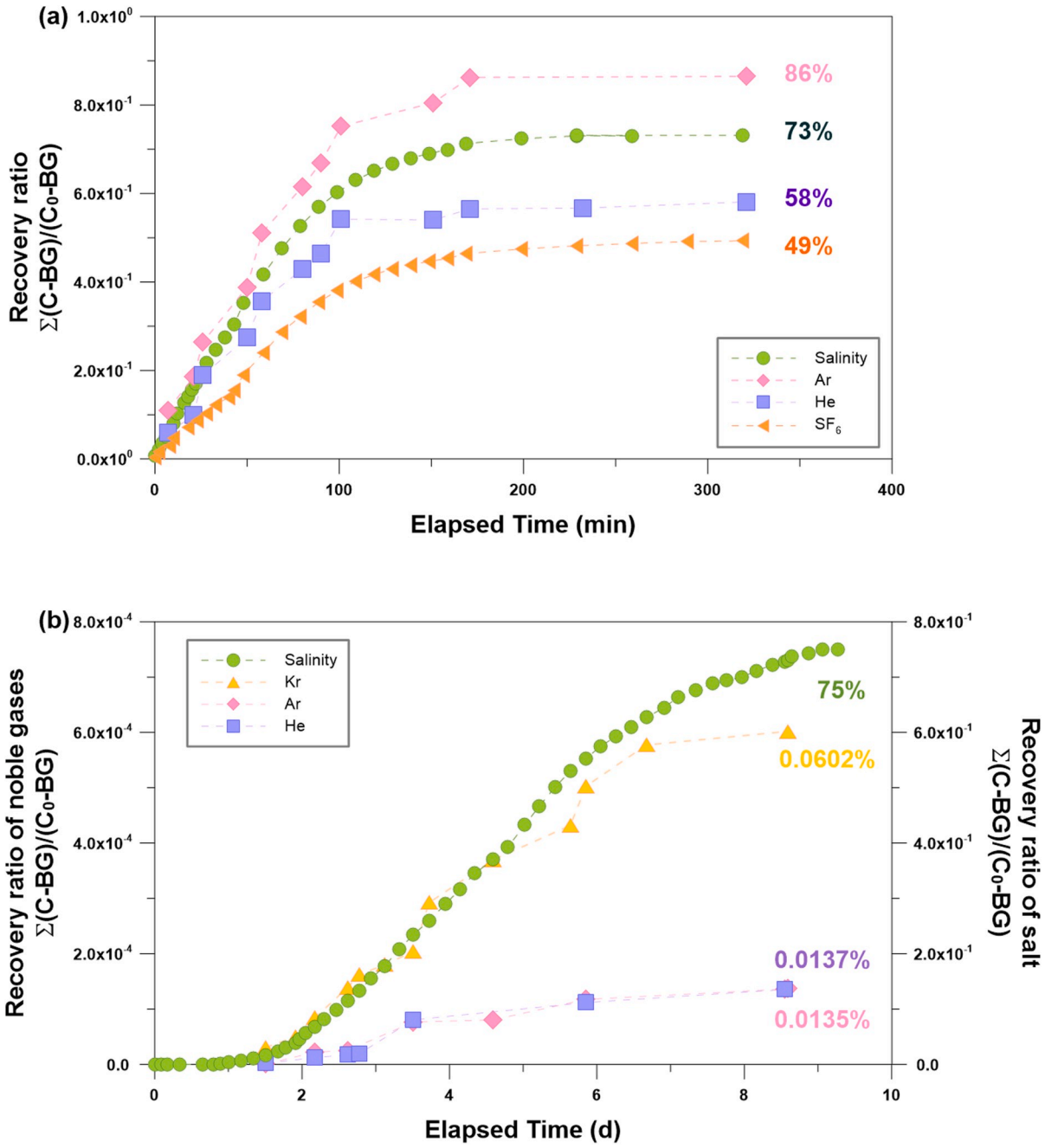

Fig. 5. Mass recovery curves of the injected tracers (a) from the SWTT and (b) from the IWTT. Each Y-axis displays the recovery ratio of tracers recorded above the background level. The recovery rate of inert gas tracers was relative to their solubility for groundwater in an air-water system, indicating that solubility-controlled processes were involved in the fate of the leaked plume.

less soluble and lighter elements are preferentially lost into the gas phase at the gas/water interfaces than those that are heavier (Ballentine et al., 2002). As shown in Fig. 6, the He/Ar changed relative to the tracer's solubility, following the degassing line (i.e., gray arrow). During the SWTT, the noble gas distribution was defined by the two physical processes such as the degassing and mixing processes. The two processes could not be explained separately, as the concentration change arose from both mechanisms occurring at the same time (Fig. 6a). This seemed to be attributable to the experimental procedure of the SWTT, in which the three-step process (push-drift-pull) caused multiple stress periods (e.g. pressure instability/vertical movement) that caused the dissolved plume to irregularly degas as the local groundwater diluted the multi-phase plume.

Two distinctive models were employed to explain the mass retention and the loss of injected tracers during the IWTT (Ballentine et al., 2002; Gilfillan et al., 2008; Ma et al., 2009). The first is the degassing of tracers in a closed system, in which air bubbles are retained and trapped in a groundwater system following the degassing process. In a closed system, equilibrium is achieved between the gas phase and the dissolved phase in the groundwater at the end of the degassing process. The second is phase-partitioning in an open system, in which the degassing process results in a mass reduction in the total mass. Consequently, air bubbles, having mobility, are lost into the atmosphere following the phase-partitioning. In an open system, the air mass is lost into the atmosphere stepwise until the end of the degassing process. Both of these extreme cases were modeled and elucidated for the fate of injected fluid during the IWTT (Appendix A). In Fig. 6b, phase-partitioning in the closed system is denoted by a gray line and that in the open system is

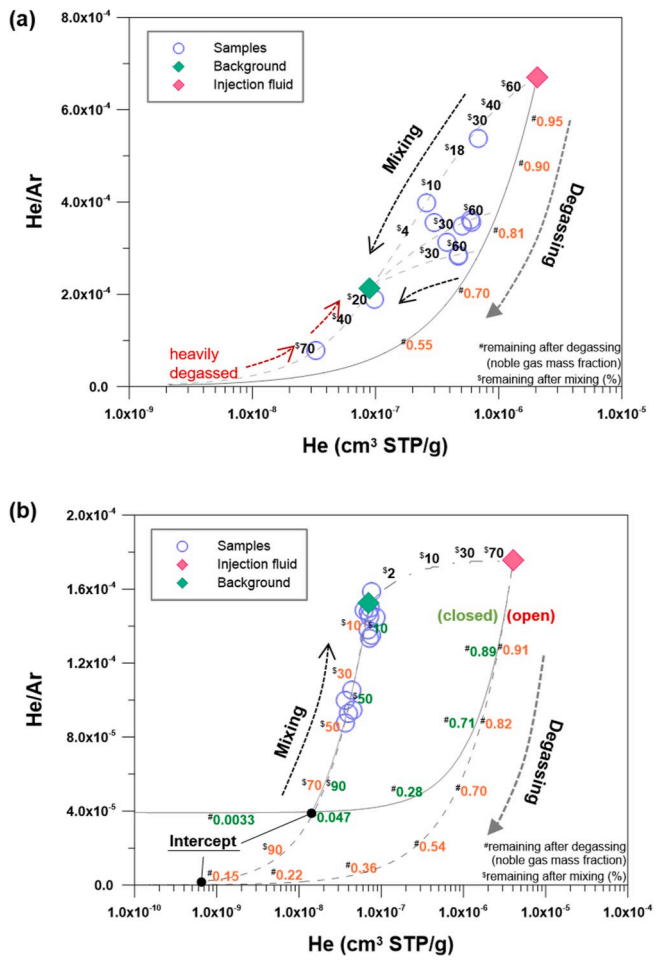

Fig. 6. (a) Noble gas concentration anomaly of the SWTT. The injected tracer changed with both the degassing and mixing processes. The two processes occurred concurrently and could not be explained separately. The heavily degassed sample spent the longest time in the groundwater system, showing the bottom upward recovery toward background levels. (b) Noble gas concentration anomaly of the IWTT. The degassing process first occurred and was followed by a mixing process. The mass retention and loss of the tracer gases can be evaluated in either an open system (orange colored) or a closed system (green colored) at the intercept (see the text for details). (For interpretation of the references to color in this figure legend, the reader is referred to the Web version of this article.)

depicted by a gray dotted line.

The two processes (i.e., degassing and mixing) were separated in the time domain during the IWTT, in which the degassing process occurred first and was followed by the mixing process, unlike in the SWTT. The separation of the two processes gave us an opportunity to quantify the degassed amount (Zhou et al., 2005). At the intercept, the gas/water ratio was 2.44 for the closed system and 0.162 for the open system. As the shallow groundwater cannot hold such a large amount of gas (gas/water = 2.44) in the system, the environment behaved like an open system during the degassing process. Then, the gas volume liberated from water was constrained at the intercept of the open system and reached 0.162×10^6 cm^3 (Fig. 6b) (Appendix A). This amount corresponds to the residual Ar of 3.61×10^{-4} cm^3 STP/g in groundwater that is already close to the ASW level (3.60×10^{-4} cm^3 STP/g) in an aquifer system, suggesting the injected plume depressurized and stabilized in the local system even before interacting with local groundwater.

4. Discussion

Noble gas tracers were employed for two injection tests to explain the physical processes involved in the migration of a leaked plume, i.e., gas-charged water, in a shallow aquifer system. During the tests, the fate of the leaked plume was first defined by a solubility-controlled process (i.e., degassing), which was followed by a volumetric mixing process. This result is consistent with observations from another artificial injection test (Ju et al., 2019), which revealed that the noble gas anomaly in a CO_2-rich plume is a function of the degassing and physical mixing processes in a shallow aquifer system (see Fig. 11 in Ju et al., 2019). Furthermore, these are similar to the conclusions reached at a natural CO_2 production site (Zhou et al., 2005) that stripping loss of insoluble gases was followed by dilution by diffusive mixing with the un-degassed local groundwater. These observations suggest that the solubility-controlled process and the mixing process are primarily responsible for the fate of the leaked plume in the shallow aquifer system.

4.1. Application of a noble gas tracer to the detection of CO_2 leakage: case study at the Weyburn and Midale oil fields

Noble gas tracers have been applied to study the fate of leaked CO_2 in a shallow aquifer system (Gilfillan et al., 2011; Ju et al., 2019; Zhou et al., 2005). However, previous studies have been sparingly applied to artificial injection tests and natural analogue sites. Although these works provide an insight on the behavior of a leaked plume, further efforts are required to link those valuable observations to an actual CCS site. Specifically, we need to know what we would observe if the free-phase CO_2 accidently reached the shallow aquifer. This can be demonstrated by simulating the hypothetical leakage on an actual CCS site based on our observations from the two distinct artificial injection tests and other valuable previous studies. To understand the fate of CO_2 under hypothetical leakage conditions, the monitoring data from the Weyburn storage site was incorporated in the leakage simulation.

The Weyburn Midale oil field is a CO_2-EOR and CO_2 storage site, where a large amount of CO_2 has been introduced into a deep reservoir (Gilfillan et al., 2017). Recently, this site received public attention as CO_2 leakage allegations implying that anthropogenic CO_2 leaked from the deep reservoir into a nearby shallow aquifer on private land were made. At this site, Gilfillan et al. (2017) used the inherent noble gas tracers in the different fluids associated with the site to judge whether upward migration had occurred from the deep reservoir into the shallow aquifer. Based on the results, the leakage allegation (i.e., upward migration of CO_2) were proved false, as the observed concentration of noble gas tracers simply did not follow the composition of the reservoir CO_2 carrying the high amount of radiogenic ^4He (see Table 1 for the composition of two reservoirs).

Though this case study proved the usefulness of a noble gas tracer, we have expanded this study in a more quantitative way to discuss what we would actually observe if free-phase CO_2 leaked into a shallow aquifer. Repeated simulations were made based on various analytical models to understand how we can use a noble gas tracer as a proxy to understand the fate of free-phase CO_2 that has leaked from a deep reservoir into a shallow aquifer system.

4.1.1. Fate of free-phase CO_2 in the shallow aquifer

Previous studies have revealed that diverse factors control the noble gas composition of captured CO_2 once it is injected into the subsurface, such as the initial capture process, degassing, dissolution, diffusion, adsorption, CO_2 density, and reservoir interactions (e.g., with atmospheric, crustal, and mantle sources) (Flude et al., 2016; Gilfillan et al., 2011; Holland and Gilfillan, 2013; Kilgallon et al., 2018; Warr et al., 2015; Wilkinson et al., 2010; Zhou et al., 2005). Furthermore, a recent artificial release test demonstrated the behavior of leaked CO_2 in a shallow aquifer, which was defined by degassing and mixing processes

Table 1
Noble gas composition in shallow groundwater and in a CO_2 plume. The noble gas distribution of dissolved CO_2 was calculated based on the composition of gas produced from the Weyburn storage reservoir. Note that the composition of the shallow aquifer is close to that of the air saturated water (ASW).

	^4He ($\times 10^{-8}$)	Ne ($\times 10^{-7}$)	^{20}Ne ($\times 10^{-7}$)	^{40}Ar ($\times 10^{-4}$)	^{36}Ar ($\times 10^{-6}$)	^{84}Kr ($\times 10^{-8}$)
Dissolved CO_2, C_0[a] (std dev.)[b]	763	0.084	0.076	0.724	0.138	1.440
	1831	0.135	0.123	0.986	0.186	0.344
	58.2	32.9	33.1	21.7	21.0	86.9
Shallow Aquifer[c]	5.84	1.90	1.73	3.04	1.03	4.92
(std dev.)[b]	29.1	18.5	18.3	9.24	8.96	11.2
ASW[d]	4.25	1.81	1.64	3.25	1.10	4.29

All the measured data were from Gilfillan et al. (2017) in cm^3/g.

[a] Noble gas contents in dissolved CO_2 prior to stripping loss calculated assuming 100% dissolution of the free-phase CO_2 at the P and T conditions of shallow groundwater; temperature of 14.3°C, salinity of 0.02 g/kg, and pressure of 0.101 MPa. The high level of ^4He in the dissolved CO_2 is attributed to an interaction between the reservoir gas and crustal sources. The depletion of the other noble gases is due to an interaction between the reservoir gas and artificially injected CO_2.

[b] 1 sigma value relative to the average (%).

[c] Average concentration of noble gases in the shallow groundwater samples.

[d] Air saturated water (ASW) concentration was calculated assuming a temperature of 14.3°C, salinity of 0.02 g/kg, and altitude of 580 m.

based on noble gas tracers (Ju et al., 2019). From the insights of previous works, we will discuss how these processes are involved in the fate of free-phase CO_2 in a shallow aquifer system based on the behavior of noble gas tracer.

The free-phase CO_2 that leaks from a deep reservoir into a shallow aquifer is rich in ^4He from previous interactions with a deep crustal source but is low in other elements from the initial industrial capture process (Table 1). Following leakage, free-phase CO_2 forms a dissolved plume in a shallow aquifer, and the contents of the plume naturally follow those of the free-phase CO_2. The concentration of the CO_2 plume (i.e., the blue cross symbol) will change in the groundwater system depending on various physical interactions, which are depicted using the ^4He and ^{40}Ar tracers in Fig. 7. A detailed description of the theoretical calculations can be found in Appendix A. One of most noticeable processes controlling the fate of this plume is a volumetric mixing process (Gilfillan et al., 2011; Ju et al., 2019) (see also Fig. 6) occurring as the CO_2 plume moves through porous media with the local groundwater. While being gradually mixed with the local groundwater, the initial plume becomes depleted in ^4He and enriched in ^{40}Ar (i.e., the black line). The noble gas anomaly in this process is dependent on the compositional difference between the initial plume and local groundwater, and their mixing fractions, whereby ^4He could vary by up to −99.6% and ^{40}Ar could vary by up to 256% (i.e., the light gray zone).

Diffusive movement occurs along the concentration gradient under Fick's second law and would be observable at the plume boundary where the CO_2 plume meets the local groundwater. This also occurs at the water table, when the plume makes contact with the atmosphere. Therefore, in these places (i.e., plume boundary and water table), the composition of the noble gas will be differentiated from that of the plume center (i.e., the red line in Fig. 7). The maximum change (%) is, however, consistent with the volumetric mixing process, as this process is also based on the concentration difference between the CO_2 plume and local groundwater. The diffusion process affects the fate of dissolved gas plume at a natural gas production site (Zhou et al., 2005). With the gas production, there was an intensive stripping loss of insoluble noble gases, which resulted in a steep concentration gradient at a contact boundary where noble gas tracers diffusively spread along a concentration gradient. In a fractured aquifer, this process can result in significant loss of insoluble noble gases into immobile zones because of a concentration gradient between the mobile (i.e., fractures) and immobile zones, and therefore, a delay of lighter elements observable at monitoring points (Carrigan et al., 1996; Sanford et al., 1996). Moreover, this behavior was minutely demonstrated in a numerical simulation following a detailed laboratory experiment (Kilgallon et al., 2018), in which the arrival time of the noble gas was determined predominantly by the diffusion process while migrating in a gas phase CO_2.

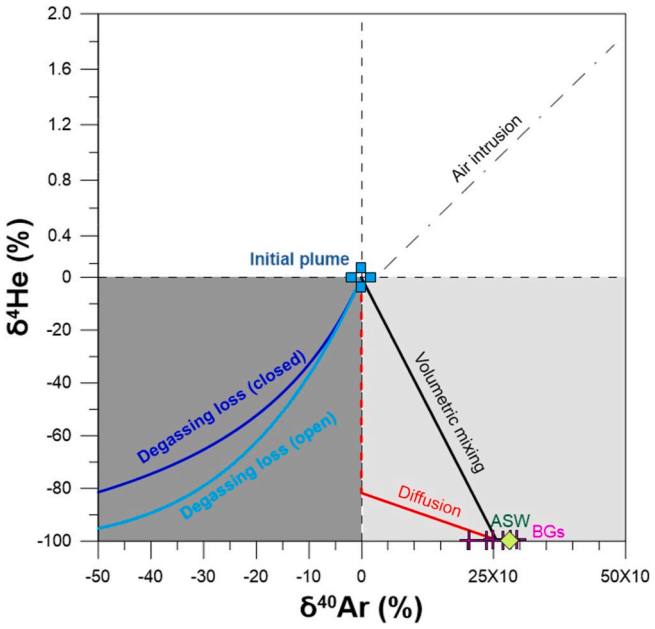

Fig. 7. Percent change in the noble gas concentration (i.e., $[NG - NG_i]/NG_i \times 100$) from the initial composition (NG_i) under various physical processes. The composition of the initial plume was calculated assuming 100% dissolution of free-phase CO_2 in the shallow aquifer (see Table 1). BGs (i.e., pink cross symbols) present the concentrations of shallow aquifer samples, and ASW is the air saturated water concentration under local groundwater conditions (i.e., green diamond; see Table 1). In the light gray zone, the mass distribution is controlled predominantly by mixing processes. Volumetric mixing occurs as the CO_2 plume moves through a porous medium with the local groundwater (i.e., the black line) (Appendix A). The diffusion process occurs along a concentration gradient, for example, at a plume boundary or water table (i.e., the red line) and is depicted with diffusion coefficients from Jähne et al. (1987) and Wise and Houghton (1966) (Eq. (A.4) in Appendix A). It only occurs at $t > 4\pi D$, theoretically (i.e., the dotted line before threshold) (Fetter, 1999). The dark gray zone indicates a large contribution of a solubility-controlled process to the fate of the CO_2 plume. The degassing process occurs during the initial period of a leakage and continues until the plume is stabilized in the relatively low pressure condition of the shallow aquifer (i.e., the blue and light blue lines) modeled using partitioning coefficients from the NIST chemistry webbook of Sander (2017) (Appendix A). Explanations for each degassing system (i.e., closed and open) can be found in the text. The air intrusion line depicts the data contamination due to the addition of atmospheric air into groundwater during the sampling procedure (i.e., the black dotted line). All the measured data were from Gilfillan et al. (2017). (For interpretation of the references to color in this figure legend, the reader is referred to the Web version of this article.)

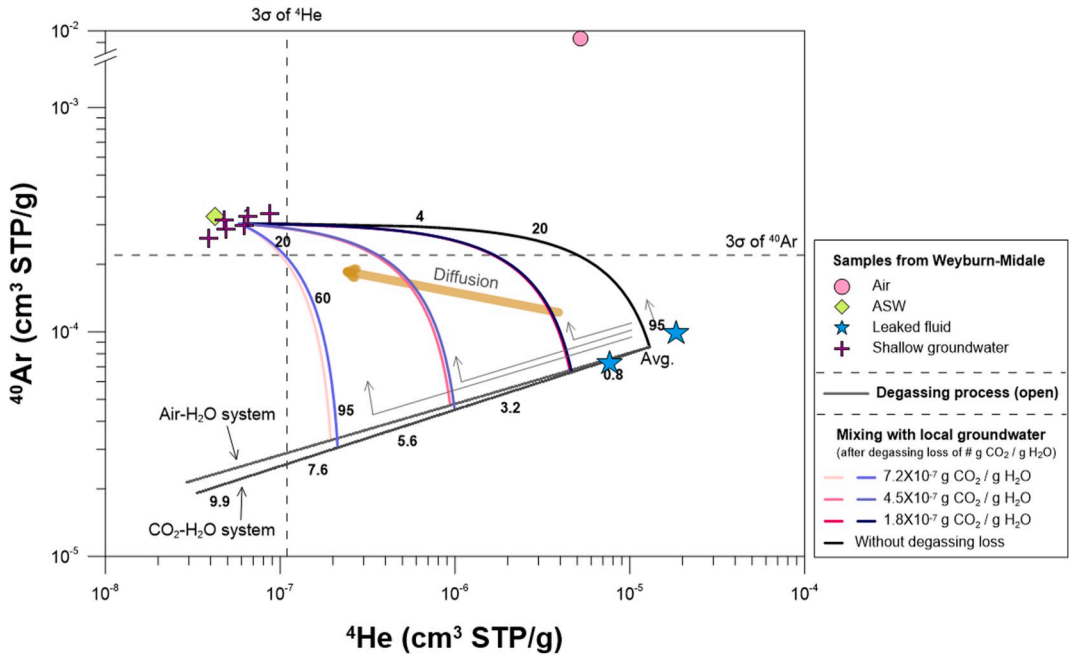

Fig. 8. Evolution of a CO_2 plume under physical processes in terms of noble gas concentration. All the measured data and hypothetical values (i.e., leaked fluid) were from Gilfillan et al. (2017). In this scenario, the initial plume is unstable and, therefore, undergoes the degassing process rapidly until stabilization is achieved in the shallow groundwater system (i.e., gray lines). Then, the degassed plume undergoes a dilution process by mixing with local groundwater (i.e., blue or pink lines). Due to the diffusion process, the points can deviate from the degassing-mixing trend and converge toward a natural background level as diluted (i.e., brown arrow), and action of this process can be prominent at the plume boundary or water table as facing a concentration gradient. From a monitoring point of view, the observed concentration will gradually evolve from the Air Saturated Water level (ASW; i.e., green diamond; see Table 1) as the CO_2 plume approaches a monitoring point, and one can eventually notice the CO_2 leakage occurrence when signals override the detection threshold, 3σ value. Note that the degassing process was depicted in both the air–H_2O system and CO_2–H_2O system (see the text for the definition of both systems). The theoretical air–H_2O system is gradually getting apart from the real CO_2–H_2O system, as degassed mass increases (see the gray lines). (For interpretation of the references to color in this figure legend, the reader is referred to the Web version of this article.)

In contrast, a solubility-controlled process leads to a depletion of all tracers (i.e., the dark gray zone in Fig. 7). This process is possibly observable at the initial stage of leakage when the CO_2 plume is unstable owing to the high partial pressure of inherent gases (Fig. 1). The initial plume would degas the CO_2 rapidly until it stabilized in the lower pressure of the shallow groundwater, as shown in the IWTT (Fig. 6b). During this process, the free CO_2 carries the insoluble gases from the dissolved phase and stays in the surrounding environment, resulting in a gas–water equilibrium (closed) or CO_2 bubbles of infinitesimally small size escaping from the groundwater continuously until the end of degassing process (open) (Ballentine et al., 2002; Gilfillan et al., 2008; Ma et al., 2009). This process results in the noble gases fractionate continuously until the plume is stabilized at local conditions of P, T, and CO_2-density in shallow groundwater. It is evident that the lighter ^4He tends to be more depleted compared to the heavier ^{40}Ar, and this trend appears more significant in the open system than in the closed system (dark gray zone). The solubility-controlled process is a major mechanism controlling the fate of a CO_2-rich plume, and has been observed in a natural analogue site of CO_2 leakage (Zhou et al., 2005) and an artificial CO_2 injection experiment (Ju et al., 2019), in addition to the current experiments.

The adsorption process is known to result in a relative enrichment of heavy noble gases (i.e., Kr and Xe) in terrigenous sediments (Fanale and Cannon, 1971), and this phenomenon is particularly noticeable in a system that includes organic rich units such as shale formation (Podosek et al., 1981). Should groundwater or free-phase CO_2 makes contact with such an organic rich formation, it will become enriched in heavier species (i.e., Kr and Xe) from the ASW composition, reflecting the release of sedimentary noble gases (i.e., heavier species) from the organic source kerogens (Torgersen et al., 2004). The action of this process has been demonstrated in organic rich sediments, where the distribution of the heavier species can be distinguished from those of a normal oil-water system (Torgersen and Kennedly, 1999) and gas-water system (Ma et al., 2009). Unfortunately, proper coefficients had not been provided for this mechanism (Holland and Gilfillan, 2013; Myers et al., 2013; Flude et al., 2016), and inevitably, an analytical calculation was not made for this process. However, groundwater that makes contact with organic matter evidently becomes enriched in heavier noble gases (i.e., Kr and Xe); therefore, samples affected by this process should be carefully treated, and lighter species (i.e., He, Ne and Ar) should be adopted for the other quantitative evaluations.

The air intrusion line depicts data contamination due to the addition of atmospheric air into groundwater during the sampling process. The effects of air contamination are very different from the other processes, as air contamination results in positive changes for both elements (i.e., the right-side of the white zone in Fig. 7). This suggests that we can possibly distinguish and separate this erroneous behavior for quantitative evaluations.

4.1.2. *Monitoring efficiency of noble gas tracers*

As noble gas analysis is time-intensive, people who want to use these tracers for monitoring CO_2 leakage will naturally wonder which tracer is most efficient. It seems evident that the tracer showing the largest compositional difference between the free-phase CO_2 and shallow system would be the most efficient for tracing CO_2 leakage in a shallow aquifer (Flude et al., 2016). In that regard, the tracer with the largest difference in concentration between the C_0 (i.e., dissolved CO_2 from Table 1) and BG (i.e., shallow aquifer from Table 1) can easily detect CO_2 in the monitoring system. In addition to the compositional difference, the natural variation is another factor controlling the monitoring efficiency. In terms of leakage monitoring, the natural variation of monitoring parameters can dilute the leakage signal and deteriorate the

Table 2
Conditions for detecting the CO_2 leakage in a monitoring system. A large difference in noble gas composition between the C_0 (i.e., dissolved CO_2 from Table 1) and the BG (i.e., shallow aquifer from Table 1) indicates a high monitoring efficiency. The CO_2 leakage will be recorded in a monitoring system for the first time when the concentration starts to increase/decrease over the 3σ value, which was calculated for each element (upper section). Each cell in bottom section indicates the minimum proportion of CO_2 plume arriving at a monitoring system needed to overcome the detection threshold (i.e., the value corresponding to the 3σ value in Fig. 8) calculated for various cases of degassing loss. Note that the large difference in ^{4}He content between the C_0 and BG will generate a huge signal that will be larger than the 3σ value with a small portion of CO_2 arriving at a monitoring point. Therefore, a high monitoring efficiency will be achieved.

	^{4}He	^{20}Ne	^{40}Ar	^{36}Ar	^{84}Kr	^{4}He/^{40}Ar	^{84}Kr/^{20}Ne
	($\times 10^{-8}$ cm^3/g)	($\times 10^{-7}$ cm^3/g)	($\times 10^{-4}$ cm^3/g)	($\times 10^{-6}$ cm^3/g)	($\times 10^{-8}$ cm^3/g)	($\times 10^{-3}$)	–
$\lvert C_0 - BG\rvert$[a]	1292	1.63	2.19	0.865	4.03	152	0.601
3σ of BG[b]	5.09	0.95	0.84	0.276	1.65	0.123	0.210
DegassingAmount[c]	mixing % with CO_2 plume[d]						
0	0.394	58.4	38.6	31.9	41.0	0.00288	5.64
1.8	1.14	56.4	35.6	30.7	40.0	0.00823	5.18
4.5	5.78	55.4	32.8	29.4	38.7	0.04	5.57
7.2	37.4	55.1	31.1	28.6	37.7	0.198	6.44

All the measured data were from Gilfillan et al. (2017).
[a] Difference in noble gas concentration between the initial CO_2 plume (C_0) and the shallow groundwater (BG). Note that a large difference indicates a high monitoring efficiency.
[b] 3 standard deviation of shallow groundwater samples, presenting the natural variability.
[c] Degassed amount from a CO_2 plume in an open system in units of $\times 10^{-7}$ cm^3 STP/g.
[d] At least n% of the CO_2 plume should arrive at the monitoring system to override the detection threshold (i.e., the 3σ value) and so that CO_2 leakage can be reported. This concept was introduced by Risk et al. (2015).

monitoring efficiency. For this complicated issue, Risk et al. (2015) defined a minimum threshold value for each monitoring parameter to confirm CO_2 leakage safely. According to previous research, a "leakage" could be detected safely when signals of a monitoring parameter increase over the three sigma value of the natural variation of the parameter. In Table 2, the threshold values (3σ) are listed for each tracer.

4.1.2.1. Physical processes affecting the monitoring efficiency. As noble gas distribution is related to physical interactions in the CO_2 leakage condition (see section 4.1.1. Fate of free-phase CO_2 in shallow aquifer), the monitoring efficiency of noble gas tracers is also dependent on physical processes. When CO_2 leakage occurs in a shallow aquifer, one can first observe the front of the CO_2 plume at a monitoring well as it gradually approaches the monitoring areas. In this case, the "first signal" of the noble gas parameters will be variable, depending on the nature and magnitude of the physical processes controlling the evolution of the CO_2-rich plume. The evolutionary path of the CO_2 plume was depicted using noble gas tracers under physical processes (Fig. 8), and was based on observations made from two iterations of artificial injection tests and previous studies (Gilfillan et al., 2011; Ju et al., 2019; Sanford et al., 1996; Zhou et al., 2005). In this scenario, the initial CO_2 plume is unstable, owing to the high partial pressure of CO_2 in the shallow aquifer (Fig. 1). Therefore, it undergoes a degassing process rapidly until it stabilizes at the shallow aquifer conditions of P, T, and CO_2-density. Then, the remaining mass (i.e., dissolved phases) undergoes a mixing process as the plume moves through the porous medium with the local groundwater toward the observation wells (Fig. 1) (Ju et al., 2019).

From a monitoring point of view, the concentrations of the noble gases will start to deviate gradually from the composition of the air saturated water (ASW) (i.e., green diamond) as the plume approaches an observation point and, at some point, they will vary over the threshold (i.e., the. 3σ line), confirming CO_2 leakage occurrence (Fig. 8). Information about the first detection points (i.e., the minimum mixing proportion of the CO_2 plume needed to override the detection limit and the composition of the noble gas tracer at this point) is listed in Table 2. For example, we can see the first arrival of ^{4}He when the CO_2 plume (1.14%) approaches a monitoring well, which initially loses a CO_2 mass of 1.8×10^{-5} CO_2 cm^3 STP/g H_2O during the degassing event.

In most cases, the ^{4}He species and their various combinations with other species showed high monitoring efficiencies than the other heavier species, which was attributed to the large amount of ^{4}He in the CO_2 plume. However, it should be noted that the efficiency of one tracer is fairly dependent on the action of the physical processes in plume migration. For example, if the CO_2 plume lost more than 7.2×10^{-5} CO_2 cm^3 STP/g H_2O during the degassing process, then ^{36}Ar and ^{40}Ar will be ahead of ^{4}He in the monitoring well (Fig. 8). Furthermore, if the diffusion process is dominant at the plume front, ^{4}He can be delayed behind other heavier species in the monitoring system because of its fast dilution along the concentration gradient, which has been demonstrated in other artificial injection tests (Carrigan et al., 1996; Sanford et al., 1996). Therefore, the detection efficiency in terms of its role as an early warning for CO_2 leakage is dependent only on the leakage conditions, and it cannot be said that any single tracer is superior to others.

4.1.2.2. Influence of density of CO_2 on the monitoring efficiency. Free-phase CO_2 forms a CO_2-rich plume in a shallow aquifer after a leakage event. The partitioning behavior of noble gas is different in pure water and in CO_2-rich plume owing to an increase in the molecular interactions inside a plume with a high CO_2 density (Warr et al., 2015). Until now, the air–H_2O partitioning coefficient has been adopted for describing the distribution of noble gas tracers in a CO-rich system instead of the CO_2–H_2O partitioning coefficient, owing to an absence of previous studies (Gilfillan et al., 2008; LaForce et al., 2014; Zhang et al.,

Table 3
Percent differences between water/gas partitioning coefficients of noble gases (top) and percent differences between noble gas concentrations in a CO_2–H_2O system and an air–H_2O system (below). The latter was calculated for various degassing events.

	^{4}He	^{40}Ar	^{84}Kr
δpartitioning[a]			
	%[a]		
	2.26	−7.32	−23.05
Degassing amount[b]	%[c]		
0	0	0	0
1.8	2.83	−2.09	−3.94
4.5	7.21	−5.15	−9.57
7.2	11.79	−8.12	−14.86

[a] Percent difference of water/gas partitioning coefficient of noble gases (unit: mM/atm) between the two systems, $(k_{i,CO2-H2O} - k_{i,air-H2O})/k_{i,air-H2O} \times 100$. Partitioning coefficients can be found in Table A1 of Appendix A.
[b] Total degassed mass in an open system (unit: $\times 10^{-7}$ cm^3 STP/g).
[c] Percent difference of concentration (unit: cm^3 STP/g) between the two systems, $(C_{i,CO2-H2O} - C_{i,air-H2O})/C_{i,air-H2O} \times 100$.

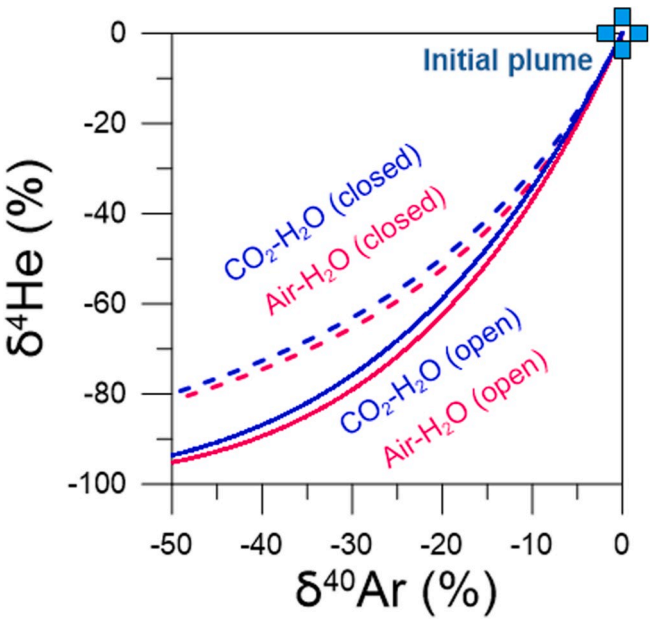

Fig. 9. Percent change in noble gas concentration from its initial composition in a CO_2 plume undergoing a degassing process for both air–H_2O and CO_2–H_2O systems. The air–H_2O system was depicted using partitioning coefficients from the NIST chemistry webbook of Sander (2017) (pink-colored), and the CO_2–H_2O system was based on coefficients from Warr et al. (2015) (blue) assuming a CO_2-saturated state (i.e., 3.97 CO_2 kg/m^3) at a temperature of 14.3°C, altitude of 580 m, and water column of 10 m (Table A1). The theoretical air–H_2O system will deviate from the real CO_2–H_2O system because molecular interactions increase with CO_2 concentration. Note that the difference between the air–H_2O (pink) and CO_2–H_2O (blue-colored) systems is smaller than the difference between the closed (dotted) and open (line) systems (see the text for definition of each system). The noble gas composition of the initial plume was from Gilfillan et al. (2017). (For interpretation of the references to color in this figure legend, the reader is referred to the Web version of this article.)

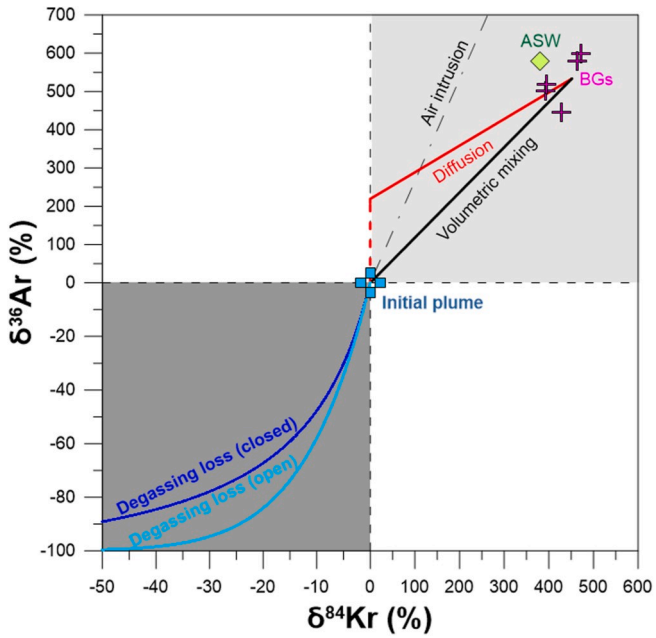

Fig. 10. Percent change in noble gas composition in the initial CO_2 plume under various physical processes. BGs (i.e., pink cross symbols) present the concentrations of shallow aquifer samples, and ASW is the air saturated water in a local groundwater condition (i.e., green diamond; see Table 1). Note that the distinction between mixing processes (i.e., the light gray zone) and solubility-controlled processes (i.e., the dark gray zone) is apparent. All the measured data were from Gilfillan et al. (2017). (For interpretation of the references to color in this figure legend, the reader is referred to the Web version of this article.)

2011). This situation caused uncertainty and errors in quantitative calculations. For example, Zhou et al. (2012) could not determine a clear reason for mismatches of heavier noble gases to the analytical model, i.e., whether it was caused by the absence of a proper coefficient (i.e., the CO_2–H_2O partitioning coefficient) or by the influence of another physical process (i.e., sedimentary excess Kr; see Fig. 12 in that paper). Then, Warr et al. (2015) pointed out the problem; specifically, the partitioning behavior of a noble gas tracer in a CO_2-rich system differs remarkably from that in an air–H_2O water system.

Under CO_2 saturation conditions, i.e., 3.97 kg/m^3 (see Table A1), the partitioning ratio of ^{4}He species to CO_2 water increased by 2.26%, but those of others decreased, e.g., by up to −7.32% for ^{40}Ar and −23.05% for ^{84}Kr (Table 3). Fig. 9 shows the percent change in noble gas concentration with a solubility-controlled process both in an air–H_2O system (pink-colored) and in a CO_2–H_2O system (blue-colored). The CO_2-rich plume will have a lower amount of heavier isotopes compared with that in the air–H_2O system, owing to the difference in water/gas partitioning coefficients between an air–H_2O system and CO_2–H_2O system (see the definition of δ partitioning in Table 3). This trend may affect the quantitative evaluation of the fate of CO_2 (Table 3). However, this effect looks relatively minor in this specific case, owing to the wide distribution of initial values (i.e., blue stars), which cancels out this trend (Fig. 8).

4.1.2.3. Optimal tracers for detecting CO_2 leakage. Although the ^{4}He tracer appears efficient in tracing the CO_2 leakage owing to its large compositional difference between the two reservoirs (Table 2), the wide variation in ascending CO_2 possibly hinders the accurate quantitative estimation. At the Weyburn site, the variation in ^{4}He distribution was 58.2% (1σ) for CO_2 (Table 1), and this was attributed to the interaction between CO_2 and crustal fluids that reside in the deep reservoir (Gilfillan et al., 2017). The scattered distribution of initial values can add errors and uncertainty to the evaluation and tracing of the fate of CO_2 (Wilkinson et al., 2010). This issue can be resolved by using atmospheric noble gases such as ^{20}Ne, ^{36}Ar, and ^{84}Kr, which have been adopted as they ignore wide variations due to interactions with reservoir fluids (Ma et al., 2009).

In Fig. 10, an anomaly of atmospheric noble gas is depicted with the various physical processes, where clear separation between the mixing (i.e., the light gray zone) and degassing processes (i.e., the dark gray zone) implies the applicability of the tracers to constraining the physical processes. However, when they are plotted together in Fig. 11 to explain the evolution of the CO_2 plume, the anomalies driven by the two processes (i.e., mixing and degassing) overlap each other within analytical error ranges and therefore one cannot differentiate one from the other. Moreover, the wide scatters of the initial values (i.e., blue stars) significantly overrode the post-anomaly of the tracers, which was contrary to the results obtained in the case where ^{4}He is combined with other components (see Fig. 8, relative to Fig. 11). Other combinations of atmospheric elements also exhibited similar problems, as illustrated in Supplementary Fig. 1. Though atmospheric components have been demonstrated to distinguish physical processes in many studies and have proved useful (Ballentine et al., 1991; Battani et al., 2000; Ma et al., 2009; Zhou et al., 2012), in this particular case, they cannot be used to determine the physical anomalies (Fig. 11 and Supplementary Fig. 1). This simulation indicated that ^{4}He and its combinations with heavier species are the most powerful proxies for understanding the fate of a CO_2 plume, as they have more distinguishable compositional changes under physical interactions than other combinations. The overall result suggests that it is mandatory to check whether the post-anomaly of a selected tracer (i.e., degassing-mixing trend) cancels out the

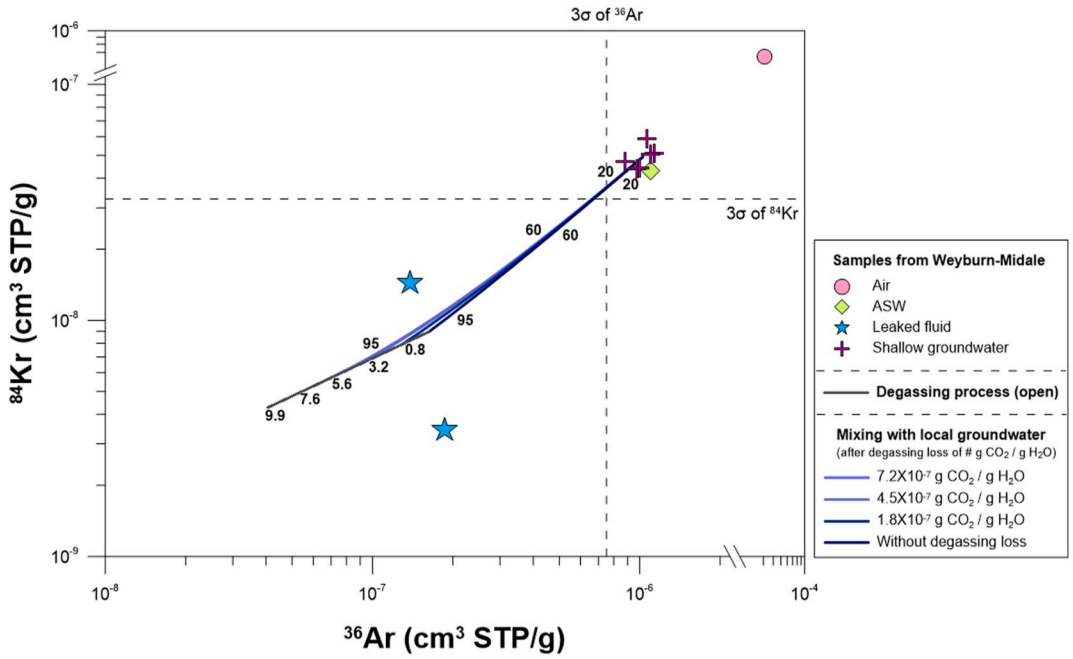

Fig. 11. Evolution of a CO_2 plume under physical processes in terms of atmospheric noble gas concentration. All the measured data were from Gilfillan et al. (2017). In this scenario, the initial plume is unstable and, therefore, undergoes a degassing process rapidly until stabilization in a shallow groundwater system is achieved (i.e., the gray line) (see Fig. 1). Then, the degassed plume undergoes a dilution process when it mixes with local groundwater (i.e., the blue lines). Note that the degassing and mixing process overlap each other and cannot be separated from the other. Furthermore, see that the wide distribution of the initial values (i.e., blue stars) cancels out the post anomaly. (For interpretation of the references to color in this figure legend, the reader is referred to the Web version of this article.)

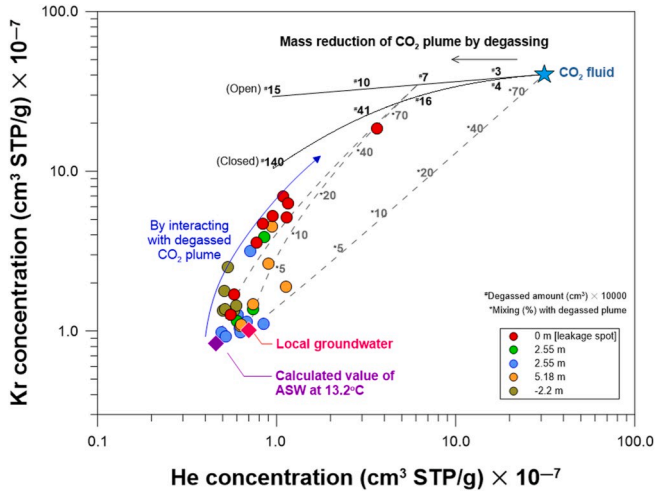

Fig. 12. He–Kr plot after CO_2 leakage into a shallow groundwater is allowed to occur; the plot was modified form Ju et al. (2019). The samples were lying on the new dilution line of the mixing trajectory between a partially degassed CO_2 plume and a background concentration (i.e., the pink/purple diamond). In other words, the samples were a mixture of the degassed CO_2 plume and the local groundwater. Note that the leakage spot (0 m; i.e., red circles) exhibited the largest variation in the mixing trajectory as the CO_2 plume interacted with the degassed CO_2 plume. The other samples were collected at a certain distance from the leakage point, and they exhibited a smaller variation. (For interpretation of the references to color in this figure legend, the reader is referred to the Web version of this article.)

heterogeneous distribution of reservoir gases.

4.2. *Identifying leakage hot spots using noble gas fingerprint in an actual CO_2 leakage site*

Accidental leakage from a deep reservoir into a shallow system can happen through various pathways, such as an injection well, an abandoned well, or natural conduits (e.g., faults or poor caprock integrity), possibly exposing CO_2 at various points in shallower groundwater. This suggests that the actual CO_2 leakage we would observe in a shallow aquifer is complicated and cannot be easily discussed with a noble gas fingerprint.

The actual CO_2 leakage can complicate the noble gas distribution as ascending CO_2 takes various paths into a shallow aquifer. However, we can still trace the CO_2 leakage by systematic and scientific investigation. In the environmental forensic world, when attempting to trace a source spot in close proximity, one can make use of an evolutionary pattern of a source compound (Morrison, 1999). Similarly, from the artificial injection tests, we also observed an evolutionary path of a leaked plume where the noble gas composition undergoes a series of modification steps owing to physical processes (i.e., degassing-mixing trend in Fig. 8). This specific trend also has been shown in the artificial CO_2 injection test in a shallow aquifer (Ju et al., 2019) and natural CO_2 production site (Zhou et al., 2005).

In terms of the evolutionary path, another representative result was demonstrated in Fig. 12 following an artificial injection of CO_2 into shallow aquifer (Ju et al., 2019) In Fig. 12, the monitoring data is plotted on the gradual trend between the degassing-end (i.e., the intercept between black line and dotted line) and the local groundwater (i.e., diamond symbols) (Ju et al., 2019). The trend indicated that the degassed plume was gradually mixed with local groundwater after the solubility-controlled process was swiftly finished. Here, the samples from a leakage spot (i.e., the red circles) exhibit the widest variation on the mixing line, which stretches from the degassing-end. This was attributed to the monitoring well, which was located at the closest point to a leakage spot and therefore efficiently captured the CO_2 plume

shortly after the degassing-end. There is a clear distinction between the source spot (i.e., wide variation) and the other monitoring wells besides the leakage spot (i.e., narrow variation around the local BG), suggesting that, with this trend, a leaking point with an actual CO_2 leakage event can potentially be identified. Therefore, the evolutionary path of the leaked plume elucidated in this study can be an important fingerprint when monitoring CO_2 leakage using a noble gas tracer.

5. Conclusions

Although noble gas tracers have been proven useful in characterizing the fate of CO_2 in many aspects of CO_2 storage research, they have not been extensively used for monitoring CO_2, i.e., to trace leaked CO_2 in shallow groundwater. Furthermore, noble gas application has been limited to the monitoring of natural analogue sites and CCS pilot test sites, suggesting we still need to link previous findings to an actual CO_2 leakage event. Therefore, this study evaluated the applicability of noble gas tracers to monitoring actual CO_2 leakage from a deep reservoir into a shallow groundwater system.

First, an artificial injection test was performed in a shallow-depth aquifer system to observe and verify observations from previous researches. Here, we used inert gas tracers (i.e., SF_6 and noble gases) to separate and explain the physical interactions that determine the fate of the leaked plume. During the tests, the fate of the leaked plume was a function of a solubility-controlled process (i.e., degassing) and a mixing process. This result was consistent with those of Ju et al. (2019) and Zhou et al. (2005), suggesting that the two processes are primarily responsible for the fate of the leaked plume in a shallow system.

While the artificial injection tests identified the major interactions responsible for the fate of the leaked plume, the applicability of tracers to actual leakage monitoring work at a CCS site has not been explored. Therefore, repeated simulations were conducted based on data from a real CO_2 injection site (the Weyburn and Midale oil fields) to predict the fate and evolutionary path of a leaked plume that we would observe with actual CO_2 leakage. This simulation indicated that ^4He and its combinations with heavier species are useful monitoring parameters for evaluating the fate of a leaked plume. In contrast, in terms of early warning of a leakage, none of the tracers were superior to the others, as their detection efficiencies appear to be dependent on the leakage conditions and therefore under the control of physical processes. Furthermore, the high density of the CO_2 of a leaked plume possibly adds uncertainty and errors to the quantitative evaluations. However, the wide scatter of the initial values (i.e., noble gas variation in produced CO_2) significantly overrides the effect of the other uncertainties in monitoring CO_2 leakage at this specific site. This suggests the homogeneity of the initial plume is significantly important in terms of the monitoring efficiency using noble gas tracers. Overall, the results of this study revealed that a noble gas can be applied not only for qualitative purposes (i.e., leaking detection), but also for identifying mass allocations and the evolutionary path of a leaked plume in a shallow aquifer system. Most importantly, the leaked plume has a unique evolutionary path in terms of noble gas tracers, which are expected to act as important fingerprints for tracing a leakage spot as complex mechanisms affect the CO_2 plume distribution.

Declaration of competing interest

The authors declare that they have no known competing financial interests or personal relationships that could have appeared to influence the work reported in this paper.

Acknowledgements

This research was supported by a Korea Environmental Industry & Technology Institute (KEITI) grant entitled “R&D Project on Environmental Management of Geologic CO2 Storage” (Project Number: 2018001810002), by a Korea Polar Research Institute grant (PE20140) and by a National Research Foundation of Korea (NRF) grant funded by the Korean government (MSIT) (NRF-2018R1C1B6007390). We thank all the members of the K-COSEM team and, appreciate Intae Kim and Minjung Kim for their efforts and support on noble gas analysis. Finally, the authors would like to thank two anonymous reviewers for their detailed comments and observations which greatly improved the present paper.

Appendix B. Supplementary data

Supplementary data to this article can be found online at https://doi.org/10.1016/j.apgeochem.2020.104609.

Appendix A. Analytical solutions for the fate of CO_2 plume

When degassing happens in a closed system, the exsolved gas will still remain in the aquifer system, and an equilibrium will be achieved at the interfaces between the bubbles and remaining plume. In this situation, one-step partitioning determines the noble gas distribution, which is defined by Henry’s constant, such as in Eq. (A.1) and Eq. (A.2) (Ballentine et al., 2002):

$$\left(\frac{A}{B}\right)_{(g)} = \left(\frac{A}{B}\right)_{(l)} \times \alpha \tag{A.1}$$

$$\alpha = \frac{\frac{r_A}{\varnothing_A} K_A}{\frac{r_B}{\varnothing_B} K_B} \tag{A.2}$$

Here:

$\left(\frac{A}{B}\right)_{(g)}$ = A and B ratio in exsolved bubbles, where A and B are different noble gases;

$\left(\frac{A}{B}\right)_{(l)}$ = the composition of A and B remaining in the dissolved phase;

α = partitioning coefficient for gas/liquid system;

K_A, K_B = Henry’s constant for A and B (Table A1);

Table A.1
Partitioning coefficients of noble gas tracers in pure water and CO_2 saturated water.

	He	Ne	Ar	Kr
	mM/atm			
Pure water†	0.389	0.482	1.711	3.211
CO_2 saturated water‡	0.398	–	1.586	2.471

†NIST chemistry webbook of Sander (2017) at temperature of 14.3°C.
‡calculated according to Warr et al. (2015) where CO_2 saturated water (3.97 kg/m^3) was assumed in temperature of 14.3°C, altitude of 580 m and water column of 10 m.

r_A, r_B = dissolved phase activity coefficients for A and B; and
$\varnothing_A$, $\varnothing_B$ = gas phase fugacity coefficients for A and B.

A Rayleigh equation was used to explain the degassing procedure in the open system, where gas bubbles continuously strip off the dissolved noble gas from the aquifer system at the gas/liquid interfaces of the exsolved bubbles until the end of the process (Ballentine et al., 2002; Zhou et al., 2005; Holland and Gilfillan, 2013).

$$\left(\frac{A}{B}\right)_{(l)} = \left(\frac{A}{B}\right)_0 \times f^{\alpha-1} \tag{A.3}$$

$\left(\frac{A}{B}\right)_{(l)}$ = The composition of A and B remaining in the aquifer
$\left(\frac{A}{B}\right)_{(0)}$ = The composition of A and B in initial CO_2 plume.
f = Fraction of element B remaining in dissolved plume.

The plume is diluted by the diffusion process in the aquifer system, along the concentration gradient between the plume and local groundwater. In dominance of this process, the distribution of noble gas element is defined by the diffusion coefficient and the elapsed time since the leakage event happened, such as in Eq. (A.4) (Fetter, 1999):

$$C = \frac{(C_0 - C_i)V}{(4\pi t)^{3/2}\sqrt{D_x D_y D_z}} \tag{A.4}$$

Here:

C = maximum concentration of element in leaked plume at a specific time, t (cm^3 STP/g);
C_0 = initial concentration of element in the leaked plume (cm^3 STP/g);
C_i = concentration of element in aquifer before leakage (cm^3 STP/g);
V = volume of the initial leaked plume (cm^3);
t = elapsed time since leakage (s); and
D_x, D_y, D_z = diffusion coefficients of element for x, y, z direction, respectively (cm^2/s) (Table A2).

Table A.2
Diffusion coefficients of noble gas tracers in water

	He	Ne	Ar‡	Kr
	cm^2/s			
Pure Water†	6.12×10^{-5}	3.23×10^{-5}	1.94×10^{-5}	1.36×10^{-5}

†Jähne et al. (1987) at temperature of 14.3°C.
‡Wise and Houghton (1966) at temperature of 14.3°C.

References

Alcalde, J., Flude, S., Wilkinson, M., Johnson, G., Edlmann, K., Bond, C.E., Scott, V., Gilfillan, S.M.V., Ogaya, X., Haszeldine, R.S., 2018. Estimating geological CO_2 storage security to deliver on climate mitigation. Nat. Commun. 9 (1), 2201. https://doi.org/10.1038/s41467-018-04423-1.

Altman, S.J., Aminzadeh, B., Balhoff, M.T., Bennett, P.C., Bryant, S.L., Cardenas, M.B., DiCarlo, D.A., Eichhubl, P., Hesse, M.A., Huh, C., Matteo, E.N., Mehmani, Y., Tenney, C.M., Yoon, H.J., 2014. Chemical and hydrodynamic mechanisms for long-term geological carbon storage. J. Phys. Chem. C 118 (28), 15103–15113. https://doi.org/10.1021/jp5006764.

Baek, W., Lee, J.Y., 2011. Source apportionment of trichloroethylene in groundwater of the industrial complex in Wonju, Korea: a 15-year dispute and perspective. Water Environ. J. 25 (3), 336–344. https://doi.org/10.1111/j.1747-6593.2010.00226.x.

Ballentine, C.J., O'nions, R.K., Oxburgh, E.R., Horvath, F., Deak, J., 1991. Rare gas constraints on hydrocarbon accumulation, crustal degassing and groundwater flow in the Pannonian Basin. Earth Planet Sci. Lett. 105 (1–3), 229–246. https://doi.org/10.1016/0012-821X(91)90133-3.

Ballentine, C.J., O'nions, R.K., 1994. The use of natural He, Ne and Ar isotopes to study hydrocarbon-related fluid provenance, migration and mass balance in sedimentary basins. Geol. Soc. Lond. Spec. Publ. 78 (1), 347–361. https://doi.org/10.1144/GSL.SP.1994.078.01.23.

Ballentine, C.J., Burgess, R., Marty, B., 2002. Tracing fluid origin, transport and interaction in the crust. In: Porcelli, D., Ballentine, C.J., Wieler, R. (Eds.), Reviews in

Mineralogy & Geochemistry Volume 47, Noble Gases in Geochemistry and Cosmochemistry, pp. 539–614.
Battani, A., Sarda, P., Prinzhofer, A., 2000. Basin scale natural gas source, migration and trapping traced by noble gases and major elements: the Pakistan Indus basin. Earth Planet Sci. Lett. 181 (1–2), 229–249. https://doi.org/10.1016/S0012-821X(00)00188-6.
Beaubien, S.E., Jones, D.G., Gal, F., Barkwith, A.K.A.P., Braibant, G., Baubron, J.C., Ciotoli, G., Graziani, S., Lister, T.R., Lombardi, S., Michel, K., Quattrocchi, F., Michel, K., 2013. Monitoring of near-surface gas geochemistry at the Weyburn, Canada, CO_2-EOR site, 2001–2011. Int. J. Greenh. Gas Control 16, 236–262. https://doi.org/10.1016/j.ijggc.2013.01.013.
Beyerle, U., Aeschbach-Hertig, W., Imboden, D.M., Baur, H., Graf, T., Kipfer, R., 2000. A mass spectrometric system for the analysis of noble gases and tritium from water samples. Environ. Sci. Technol. 34 (10), 2042–2050. https://doi.org/10.1021/es990840h.
Bosch, A., Mazor, E., 1988. Natural gas association with water and oil as depicted by atmospheric noble gases: case studies from the southeastern Mediterranean Coastal Plain. Earth Planet Sci. Lett. 87 (3), 338–346. https://doi.org/10.1016/0012-821X(88)90021-0.
Carrigan, C.R., Heinle, R.A., Hudson, G.B., Nitao, J.J., Zucca, J.J., 1996. Trace gas emissions on geological faults as indicators of underground nuclear testing. Nature 382 (6591), 528–531.
Chen, M., Park, M., Kim, J.H., Shinn, Y.J., Lee, Y.K., Hur, J., 2018. Exploring pore water biogeochemical characteristics as environmental monitoring proxies for a CO_2 storage project in Pohang Basin, South Korea. Mar. Pollut. Bull. 137, 331–338. https://doi.org/10.1016/j.marpolbul.2018.10.036.
Cohen, G., Loisy, C., Laveuf, C., Le Roux, O., Delaplace, P., Magnier, C., Rouchon, V., Garcia, B., Cerepi, A., 2013. The CO_2-Vadose project: experimental study and modelling of CO_2 induced leakage and tracers associated in the carbonate vadose zone. Int. J. Greenh. Gas Control 14, 128–140. https://doi.org/10.1016/j.ijggc.2013.01.008.
Fanale, F.P., Cannon, W.A., 1971. Physical adsorption of rare gases on terrigenous sediments. Earth Planet Sci. Lett. 11, 362–368.
Fetter, C.W., 1999. Contaminant Hydrogeology, second ed. Prentice-Hall, New York, pp. 70–74.
Flude, S., Johnson, G., Gilfillan, S.M., Haszeldine, R.S., 2016. Inherent tracers for carbon capture and storage in sedimentary formations: composition and applications. Environ. Sci. Technol. 50 (15), 7939–7955. https://doi.org/10.1021/acs.est.6b01548.
Gilfillan, S.M.V., Ballentine, C.J., Holland, G., Blagburn, D., Sherwood Lollar, B., Scott, S., Schoell, M., Cassidy, M., 2008. The noble gas geochemistry of natural CO_2 gas reservoirs from the Colorado Plateau and Rocky Mountain provinces, USA. Geochem. Cosmochim. Acta 72, 1174–1198. https://doi.org/10.1016/j.gca.2007.10.009.
Gilfillan, S.M.V., Lollar, B.S., Holland, G., Blagburn, D., Stevens, S., Schoell, M., Cassidy, M., Ding, Z., Zhou, Z., Lacrampe-Couloume, G., Ballentine, C.J., 2009. Solubility trapping in formation water as dominant CO_2 sink in natural gas fields. Nature 458 (7238), 614–618. https://doi.org/10.1016/j.gca.2007.10.009.
Gilfillan, S.M.V., Wilkinson, M., Haszeldine, R.S., Shipton, Z.K., Nelson, S.T., Poreda, R.J., 2011. He and Ne as tracers of natural CO_2 migration up a fault from a deep reservoir. Int. J. Greenh. Gas Control 5 (6), 1507–1516. https://doi.org/10.1016/j.ijggc.2011.08.008.
Gilfillan, S.M.V., Sherk, G.W., Poreda, R.J., Haszeldine, R.S., 2017. Using noble gas fingerprints at the Kerr Farm to assess CO_2 leakage allegations linked to the Weyburn-Midale CO_2 monitoring and storage project. Int. J. Greenh. Gas Control 63, 215–225. https://doi.org/10.1016/j.ijggc.2017.05.015.
Györe, D., Stuart, F.M., Gilfillan, S.M.V., Waldron, S., 2015. Tracing injected CO_2 in the Cranfield enhanced oil recovery field (MS, USA) using He, Ne and Ar isotopes. Int. J. Greenh. Gas Control 42, 554–561. https://doi.org/10.1016/j.ijggc.2015.09.009.
Györe, D., Gilfillan, S.M.V., Stuart, F.M., 2017. Tracking the interaction between injected CO_2 and reservoir fluids using noble gas isotopes in an analogue of large-scale carbon capture and storage. Appl. Geochem. 78, 116–128. https://doi.org/10.1016/j.apgeochem.2016.12.012.
Györe, D., McKavney, R., Gilfillan, S.M.V., Stuart, F.M., 2018. Fingerprinting coal-derived gases from the UK. Chem. Geol. 480, 75–85. https://doi.org/10.1016/j.chemgeo.2017.09.016.
Heilweil, V.M., Solomon, D.K., Perkins, K.S., Ellett, K.M., 2004. Gas-partitioning tracer test to quantify trapped gas during recharge. Ground Water 42 (4), 589–600. https://doi.org/10.1111/j.1745-6584.2004.tb02627.x.
Holland, G., Gilfillan, S., 2013. Application of noble gases to the viability of CO_2 storage. In: Burnard, P. (Ed.), The Noble Gases as Geochemical Tracers. Advances in Isotope Geochemistry. Springer, Berlin, Heidelberg, pp. 177–223. https://doi.org/10.1007/978-3-642-28836-4_8.
IPCC, 2005. In: Metz, B., Davidson, O., de Coninck, H.C., Loos, M., Meyer, L.A. (Eds.), IPCC Special Report on Carbon Dioxide Capture and Storage, Prepared by Working Group III of the Intergovernmental Panel on Climate Change. Cambridge University Press, Cambridge, United Kingdom/New York, NY, USA, pp. 208–210.
Jähne, B., Heinz, G., Dietrich, W., 1987. Measurement of the diffusion coefficients of sparingly soluble gases in water. J. Geophys. Res.: Oceans 92 (C10), 10767–10776. https://doi.org/10.1029/JC092iC10p10767.
Ju, Y., Beaubien, S.E., Lee, S.S., Kaown, D., Hahm, D., Lee, S., Park, I.W., Park, K., Yun, S.T., Lee, K.K., 2019. Application of natural and artificial tracers to constrain CO_2 leakage and degassing in the K-COSEM site, South Korea. Int. J. of Greenh. Gas Control 86, 211–225. https://doi.org/10.1016/j.ijggc.2019.05.002.
Ju, Y., Lee, S.S., Kaown, D., Lee, K.K., 2018. Application of Inert Gas Tracers to Identify the Physical Processes Governing the Mass Balance Problem of Leaking CO_2 in Shallow Groundwater System. In: 14th Greenhouse Gas Control Technologies Conference. Melbourne; Australia; October 21–26. https://papers.ssrn.com/sol3/papers.cfm?abstract_id=3365686.
Ju, Y., Kaown, D., Lee, K.K., 2018b. A three-pronged approach for identifying source and extent of nitrate contamination in groundwater. J. Soil Water Conserv. 73 (5), 493–503. https://doi.org/10.2489/jswc.73.5.493.
Jung, N.H., Han, W.S., Han, K., Park, E., 2015. Regional-scale advective, diffusive, and eruptive dynamics of CO_2 and brine leakage through faults and wellbores. J. Geophys. Res. Solid Earth 120 (5), 3003–3025. https://doi.org/10.1002/2014JB011722.
Kaown, D., Shouakar-Stash, O., Yang, J., Hyun, Y., Lee, K.K., 2014. Identification of multiple sources of groundwater contamination by dual isotopes. Ground Water 52 (6), 875–885. https://doi.org/10.1111/gwat.12130.
Kilgallon, R., Gilfillan, S.M.V., Edlmann, K., McDermott, C.I., Naylor, M., Haszeldine, R.S., 2018. Experimental determination of noble gases and SF_6, as tracers of CO_2 flow through porous sandstone. Chem. Geol. 480, 93–104. https://doi.org/10.1016/j.chemgeo.2017.09.022.
Kim, H.H., Lee, S.S., Ha, S.W., Lee, K.K., 2018. Application of single-well push-drift-pull tests using dual tracers (SF_6 and salt) for designing CO_2 leakage monitoring network at the Environmental Impact Test site in Korea. Geosci. J. 22 (6), 1041–1052. https://doi.org/10.1007/s12303-018-0045-9.
Kim, H.H., Koh, E.H., Lee, S.S., Lee, K.K., 2019. Biased estimation of groundwater velocity from a push-pull tracer test due to plume density and pumping rate. Water 11 (8), 1558. https://doi.org/10.3390/w11081558.
Koo, C.M., Lee, K., Kim, M., Kim, D.O., 2005. Automated system for fast and accurate analysis of SF_6 injected in the surface ocean. Environ. Sci. Technol. 39 (21), 8427–8433. https://doi.org/10.1021/es050149g.
LaForce, T., Ennis-King, J., Boreham, C., Paterson, L., 2014. Residual CO_2 saturation estimate using noble gas tracers in a single-well field test: the CO2CRC Otway project. Int. J. Greenh. Gas Control 26, 9–21. https://doi.org/10.1016/j.ijggc.2014.04.009.
Lafortune, S., Moreira, M., Agrinier, P., Bonneville, A., Schneider, H., Catalette, H., 2009. Noble gases as tools for subsurface monitoring of CO2 leakage. Energy Procedia 1 (1), 2185–2192. https://doi.org/10.1016/j.egypro.2009.01.284.
Lee, K.K., Ellsworth, W.L., Giardini, D., Townend, J., Ge, S., Shimamoto, T., Yeo, I.W., Kang, T.S., Rhie, J., Sheen, D.H., Chang, C., Woo, J.U., Langenbruch, C., 2019. Managing injection-induced seismic risks. Science 364 (6442), 730–732. https://doi.org/10.1126/science.aax1878.
Lee, K.K., Lee, S.H., Yun, S.T., Jeen, S.W., 2016. Shallow groundwater system monitoring on controlled CO_2 release sites: a review on field experimental methods and efforts for CO_2 leakage detection. Geosci. J. 20 (4), 569–583. https://doi.org/10.1007/s12303-015-0060-z.
Lee, S.S., Ju, Y., Ha, S.W., Joun, W.T., Jun, S.C., Yun, S.T., Lee, K.K., 2018. Controlled CO_2 injection into a shallow aquifer and leakage detection monitoring by two different leakage events at the K-cosem site, Korea. In: 14th Greenhouse Gas Control Technologies Conference Melbourne. Australia; October 21–26. https://papers.ssrn.com/sol3/papers.cfm?abstract_id=3366360.
Lee, S.S., Kaown, D., Lee, K.K., 2015. Evaluation of the fate and transport of chlorinated ethenes in a complex groundwater system discharging to a stream in Wonju, Korea. J. Contam. Hydrol. 182, 231–243. https://doi.org/10.1016/j.jconhyd.2015.09.005.
Lee, S.S., Kim, H.H., Joun, W.T., Lee, K.K., 2017. Design and construction of groundwater monitoring network at shallow-depth CO_2 injection and leak test site, Korea. Energy Procedia 114, 3060–3069. https://doi.org/10.1016/j.egypro.2017.03.1434.
Lollar, B.S., Ballentine, C.J., Onions, R.K., 1997. The fate of mantle-derived carbon in a continental sedimentary basin: integration of C/He relationships and stable isotope signatures. Geochem. Cosmochim. Acta 61 (11), 2295–2307. https://doi.org/10.1016/S0016-7037(97)00083-5.
Lott, D.E., Jenkins, W.J., 1998. Advances in analysis and shipboard processing of tritium and helium samples. Int. WOCE Newsl. 30, 27–30.
Lu, J., Cook, P.J., Hosseini, S.A., Yang, C., Romanak, K.D., Zhang, T., Freifeld, B.M., Smyth, R.C., Zeng, H., Hovorka, S.D., 2012. Complex fluid flow revealed by monitoring CO_2 injection in a fluvial formation. J. Geophys. Res. Solid Earth 117, B03208. https://doi.org/10.1029/2011JB008939.
Ma, L., Castro, M.C., Hall, C.M., 2009. Atmospheric noble gas signatures in deep Michigan Basin brines as indicators of a past thermal event. Earth Planet Sci. Lett. 277 (1–2), 137–147. https://doi.org/10.1016/j.epsl.2008.10.015.
Morrison, R.D., 1999. Environmental Forensics: Principles and Applications. CRC, Boca Raton, FL, pp. 209–242.
Myers, M., Stalker, L., Pejcic, B., Ross, A., 2013. Tracers–Past, present and future applications in CO_2 geosequestration. Appl. Geochem. 30, 125–135. https://doi.org/10.1016/j.apgeochem.2012.06.001.
Pinti, D.L., Marty, B., 1995. Noble gases in crude oils from the Paris Basin, France: implications for the origin of fluids and constraints on oil-water-gas interactions. Geochem. Cosmochim. Acta 59 (16), 3389–3404. https://doi.org/10.1016/0016-7037(95)00213-J.
Podosek, F.A., Bernatowicz, T.J., Kramer, F.E., 1981. Adsorption of xenon and krypton on shales. Geochem. Cosmochim. Acta 45 (12), 2401–2415. https://doi.org/10.1016/0016-7037(81)90094-6.
Prinzhofer, A., 2013. Noble gases in oil and gas accumulations. In: Burnard, P. (Ed.), Noble Gases as Geochemical Tracers. Springer, New York, pp. 225–247.
Rillard, J., Loisy, C., Le Roux, O., Cerepi, A., Garcia, B., Noirez, S., Rouchon, V., Delaplaceb, P., Willequet, O., Bertrand, C., 2015. The DEMO-CO_2 project: a vadose zone CO_2 and tracer leakage field experiment. Int. J. Greenh. Gas Control 39, 302–317. https://doi.org/10.1016/j.ijggc.2015.04.012.
Risk, D., Lavoie, M., Nickerson, N., 2015. Using the Kerr investigations at Weyburn to screen geochemical tracers for near-surface detection and attribution of leakage at

CCS/EOR sites. Int. J. Greenh. Gas Control 35, 13–17. https://doi.org/10.1016/j.ijggc.2015.01.019.

Sander, R., 2017. Henry's law constants. In: Linstrom, P.J., Mallard, W.G. (Eds.), NIST Chemistry WebBook, NIST Standard Reference Database Number 69. National Institute of Standards and Technology, Gaithersburg MD. https://doi.org/10.18434/T4D303, 20899.

Sanford, W.E., Shropshire, R.G., Solomon, D.K., 1996. Dissolved gas tracers in groundwater: simplified injection, sampling, and analysis. Water Resour. Res. 32 (6), 1635–1642. https://doi.org/10.1029/96WR00599.

Stalker, L., Boreham, C., Underschultz, J., Freifeld, B., Perkins, E., Schacht, U., Sharma, S., 2015. Application of tracers to measure, monitor and verify breakthrough of sequestered CO_2 at the CO2CRC Otway Project, Victoria, Australia. Chem. Geol. 399, 2–19. https://doi.org/10.1016/j.chemgeo.2014.12.006.

Stanley, R.H., Jenkins, W.J., Lott, D.E., Doney, S.C., 2009. Noble gas constraints on air-sea gas exchange and bubble fluxes. J. Geophys. Res.: Oceans 114 (C11), C11020. https://doi.org/10.1029/2009JC005396.

Torgersen, T., Kennedy, B.M., 1999. Air-Xe enrichments in Elk Hills oil field gases: role of water in migration and storage. Earth Planet Sci. Lett. 167 (3–4), 239–253. https://doi.org/10.1016/S0012-821X(99)00021-7.

Torgersen, T., Kennedy, B.M., van Soest, M.C., 2004. Diffusive separation of noble gases and noble gas abundance patterns in sedimentary rocks. Earth Planet Sci. Lett. 226 (3–4), 477–489. https://doi.org/10.1016/j.epsl.2004.07.030.

Warr, O., Rochelle, C.A., Masters, A., Ballentine, C.J., 2015. Determining noble gas partitioning within a CO_2–H_2O system at elevated temperatures and pressures. Geochem. Cosmochim. Acta 159, 112–125. https://doi.org/10.1016/j.gca.2015.03.003.

Whiticar, M.J., 1999. Carbon and hydrogen isotope systematics of bacterial formation and oxidation of methane. Chem. Geol. 161 (1–3), 291–314. https://doi.org/10.1016/S0009-2541(99)00092-3.

Wilkinson, M., Gilfillan, S.M.V., Haszeldine, R.S., Ballentine, C.J., 2010. Plumbing the depths: testing natural tracers of subsurface CO_2 origin and migration, Utah. In: Grobe, M., Pashin, J.C., Dodge, R.L. (Eds.), Arbon Dioxide Sequestration in Geological Media – State of the Science, C, vol. 59. American Association of Petroleum Geologists Studies, pp. 619–634. https://doi.org/10.1306/13171266St591353.

Wise, D.L., Houghton, G., 1966. The diffusion coefficients of ten slightly soluble gases in water at 10–60^oC. Chem. Eng. Sci. 21 (11), 999–1010. https://doi.org/10.1016/0009-2509(66)85096-0.

Yu, S.Y., Chae, G.T., Jeon, K.H., Jeong, J.S., Park, J.G., 2006. Trichloroethylene contamination in fractured bedrock aquifer in Wonju, South Korea. Bull. Environ. Contam. Toxicol. 76 (2), 341–348. https://doi.org/10.1007/s00128-006-0927-9.

Zhang, Y., Freifeld, B., Finsterle, S., Leahy, M., Ennis-King, J., Paterson, L., Dance, T., 2011. Single-well experimental design for studying residual trapping of supercritical carbon dioxide. Int. J. Greenh. Gas Control 5 (1), 88–98. https://doi.org/10.1016/j.ijggc.2010.06.011.

Zhou, Z., Ballentine, C.J., Kipfer, R., Schoell, M., Thibodeaux, S., 2005. Noble gas tracing of groundwater/coalbed methane interaction in the San Juan Basin, USA. Geochem. Cosmochim. Acta 69 (23), 5413–5428. https://doi.org/10.1016/j.gca.2005.06.027.

Zhou, Z., Ballentine, C.J., Schoell, M., Stevens, S.H., 2012. Identifying and quantifying natural CO_2 sequestration processes over geological timescales: the Jackson Dome CO2 Deposit, USA. Geochem. Cosmochim. Acta 86, 257–275. https://doi.org/10.1016/j.gca.2012.02.028.

Ide, S.T., Friedmann, S.J., Herzog, H.J., 2006. CO2 leakage through existing wells: current technology and regulations. In 8th International Conference on Greenhouse Gas Control Technologies 19–22.